

Overview of the Physics and Engineering Design of NSTX Upgrade

J.E. Menard¹, M. Bell¹, J. Bialek², J. Canik³, J. Chrzanowski¹,
M. Denault¹, L. Dudek¹, D.A. Gates¹, S. Gerhardt¹,
W. Guttenfelder¹, R. Hatcher¹, R. Kaita¹, S. Kaye¹, C. Kessel¹,
E. Kolemen¹, H. Kugel¹, R. Maingi³, M. Mardenfeld¹,
D. Mueller¹, B. Nelson⁴, C. Neumeyer¹, M. Ono¹, E. Perry¹,
R. Ramakrishnan¹, R. Raman⁴, S. Sabbagh¹, M. Smith¹,
V. Soukhanovskii⁵, T. Stevenson¹, R. Strykowski¹, P. Titus¹,
K. Tresemer¹, M. Viola¹, M. Williams¹, R. Woolley¹,
A. Zolfaghari¹, and the NSTX Team

¹Princeton Plasma Physics Laboratory, Princeton, NJ, USA

²Columbia University, New York, NY, USA

³Oak Ridge National Laboratory, Oak Ridge, TN, USA

⁴University of Washington, Seattle, WA, USA

⁵Lawrence Livermore National Laboratory, Livermore, CA, USA

Abstract. The spherical tokamak (ST) is a leading candidate for a fusion nuclear science facility (FNSF) due to its compact size and modular configuration. The National Spherical Torus eXperiment (NSTX) is a MA-class ST facility in the U.S. actively developing the physics basis for an ST-based FNSF. In plasma transport research, ST experiments exhibit a strong (nearly inverse) scaling of normalized confinement with collisionality, and if this trend holds at low collisionality, high fusion neutron fluences could be achievable in very compact ST devices. A major motivation for the NSTX Upgrade (NSTX-U) is to span the next factor of 3-6 reduction in collisionality. To achieve this collisionality reduction with equilibrated profiles, NSTX-U will double the toroidal field, plasma current, and NBI heating power and increase the pulse length from 1-1.5s to 5s. In the area of stability and advanced scenarios, plasmas with higher aspect ratio and elongation, high β_N , and broad current profiles approaching those of an ST-based FNSF have been produced in NSTX using active control of the plasma β and advanced resistive wall mode control. High non-inductive current fractions of 70% have been sustained for many current diffusion times, and the more tangential injection of the 2nd NBI of the Upgrade is projected to increase the NBI current drive by up to a factor of 2 and support 100% non-inductive operation. More tangential NBI injection is also projected to provide non-solenoidal current ramp-up as needed for an ST-based FNSF. In boundary physics, NSTX measures an inverse relationship between the scrape-off layer heat-flux width and plasma current that could unfavorably impact next-step devices. Recently, NSTX has successfully demonstrated substantial heat-flux reduction using a snowflake divertor configuration, and this type of divertor is incorporated in the NSTX-U design. The physics and engineering design supporting NSTX Upgrade is described.

PACS numbers: 28.52.Av, 52.25.Fi, 52.55.Fa, 52.55.Rk, 52.55.Wq

1. Introduction

The spherical tokamak (ST) [1, 2] is a leading candidate for a Fusion Nuclear Science Facility (FNSF) due to its compact size and modular configuration [3, 4]. The National Spherical Torus eXperiment (NSTX) [5, 6] is a MA-class ST facility in the U.S. actively developing the physics basis for an ST-based FNSF. Access to low collisionality ν^* plasmas in the ST configuration is particularly important to more fully understand transport, stability, and non-inductive start-up and sustainment in the spherical torus/tokamak (ST). In particular, NSTX [7] and MAST [8, 9] observe a strong inverse scaling of normalized confinement with ν^* . An example of this scaling is shown in Figure 1 for NSTX experiments in which the plasma q , β , and ρ_* were approximately fixed as the electron collisionality ν_e^* was varied by a factor of 3. If the strong favorable scaling of increased dimensionless confinement $\Omega_i \tau_E \propto B_T \tau_E$ with reduced collisionality holds at low collisionality, high fusion neutron fluxes and fluences could be achievable in very compact ST devices only 30-50% larger in major radius than existing ST devices, thereby enabling a reduced size and cost ST-based Fusion Nuclear Science Facility (ST-FNSF).

For ST high-power H-mode plasmas, the electron and ion thermal diffusivities are found to have different scaling dependencies [10]. In particular, the ion confinement is typically near neoclassical values in the outer half of the plasma minor radius and has a nearly linear plasma current dependence. In contrast, the electron confinement is anomalous and has a nearly linear toroidal field dependence. Several instabilities potentially responsible for anomalous electron thermal transport have been studied in NSTX including Electron Temperature Gradient (ETG) modes [11, 12, 13, 14, 15], Global Alfvén Eigenmodes (GAE) [16, 17], and micro-tearing modes [18, 19, 20, 21].

Unraveling the simultaneous effects of these instabilities is a major research goal of NSTX Upgrade by extending the achievable collisionality, toroidal field, and plasma current. For example, ETG-driven anomalous diffusivity is expected to depend on magnetic field strength through the electron larmor radius scaling [22] (and possibly on β), the GAE instability drive [17] is expected to depend on the fast ion velocity normalized to the Alfvén speed, the fast-ion β fraction, and the fast-ion distribution function anisotropy, and micro-tearing-induced anomalous transport is expected to depend on collisionality and also on magnetic field strength through electron larmor radius scaling [19].

As shown in Figure 2, recent nonlinear gyrokinetic simulations of micro-tearing-

induced electron transport [21] (which do not yet account for the equilibrium $E \times B$ shear) have shown reasonable agreement with experimentally inferred electron thermal diffusivities for the limited range of shots and minor radii tested. These simulations indicate that micro-tearing-induced electron transport should continue to scale nearly linearly with collisionality over approximately one order of magnitude in collisionality as the collisionality is reduced below present NSTX values. Thus, collisionality variation could impact which type(s) of instabilities dominate anomalous electron transport in NSTX Upgrade plasmas. Beyond impacting turbulent transport, reduced collisionality could also impact toroidal rotation damping [23, 24, 25], RWM stability [25, 26], error-field correction [27, 28], pedestal stability [29], and many other physics areas.

To improve the understanding of ST confinement, stability, and other physics, a major upgrade to NSTX is planned to span the next factor of 3-6 reduction in collisionality while also extending ST physics regimes and capabilities including fully non-inductive current ramp-up and sustainment. The physics and engineering design of NSTX Upgrade is described in detail in Section 2 and is summarized in Section 3.

2. Physics Requirements and Engineering Design

2.1. Centerstack, PF coils, Structural Enhancements

2.1.1. Physics Requirements Overview Scoping studies of NSTX-U operating scenarios are important for identifying the Upgrade performance requirements to achieve the physics research goals. Using 0-D scaling analysis benchmarked against NSTX experimental data, Table 1 contains parameters of interest for an NSTX reference discharge and for several representative NSTX-U scenarios assuming two confinement scalings: ITER IPB98(y,2) H-mode scaling [30, 31] and an ST-specific confinement scaling based on combined NSTX and MAST scalings: $\tau_E \propto I_p^{0.6} B_T^{1.2} n^{0.2} P^{-0.7} R^2 \epsilon^{0.6}$. Further, parameters are shown for two assumed plasma densities: 0.5 and 1.0 times the Greenwald density limit [32, 33]. The representative NSTX-U operating scenarios include: 100% non-inductive current drive, partially-inductively-driven long-pulse, high/maximum plasma current, and high current plus high heating power. These scenarios address critical issues for the ST, namely: non-inductive sustainment, the establishment of equilibrated integrated scenarios, ST confinement and stability scaling and understanding, and high-power and particle exhaust understanding and mitigation, respectively.

With respect to collisionality reduction relative to the NSTX reference scenario, a

factor of 5-6 decrease in collisionality is projected to be achievable at fixed Greenwald fraction by operating at 1T, 1.25MA, and 6MW assuming ST confinement scaling (right-most green columns). This strong decrease in collisionality at current and power values similar to the present NSTX is the result of the strong toroidal field dependence of the ST confinement scaling. In contrast, if ITER H-mode confinement scaling is assumed, only a factor of 2-3 reduction in collisionality would be achieved even with 2 times higher current and/or power (red and left-most green columns) due to the weak toroidal field dependence of the ITER confinement scaling. Thus, the ability to double the toroidal field, plasma current, and heating power is needed to reduce the uncertainty in the scaling of ST energy confinement as plasma temperatures are increased toward the values of next-step STs.

The required coil and plasma current pulse duration is another important consideration, and here the current redistribution time is generally the longest profile relaxation time-scale. On NSTX, 3-4 current redistribution times are typically required to achieve an equilibrated q profile, and if confinement continues to scale nearly inversely with collisionality at low collisionality, the current redistribution time could increase as much as a factor of 5 (compare right-most green columns to NSTX reference). Thus, to ensure similar profile relaxation in the Upgrade, the plasma current and TF flat-top durations must increase by a factor of 5 to 5s and 6.6s respectively.

2.1.2. Ohmic heating solenoid flux requirements To assess ST physics at 2 times higher TF and similar safety factor q, the plasma current must double from 1MA to 2MA. Sufficient loop voltage must also be provided for any needed inductive current drive. The operating scenario analysis indicates that 2MA plasmas at intermediate power levels (10MW) assuming ITER confinement scaling and Greenwald fraction of 1 require the highest surface voltage (0.2-0.25V) for sustainment, and these scenarios determine the required OH flux to sustain a 5s plasma current flat-top.

In addition to the flat-top flux, plasma initiation and current ramp-up are also important considerations for specifying the OH flux requirement. For plasma initiation/breakdown, the magnetic null quality and/or toroidal electric field must be sufficiently high for the plasma electron avalanche to occur to form a closed flux surface tokamak configuration. A key metric for plasma breakdown is the electron energy gained before loss to the surrounding walls via parallel transport along the total (toroidal + poloidal) background magnetic field, and this gain is proportional to the Lloyd parameter $E_\phi B_\phi / B_\perp$ [34]. The NSTX Lloyd parameter is typically 4.2kV/m at the major radius of

the centerstack where plasma breakdown is initiated ($R_{BD}=0.185\text{m}$) for a stray poloidal field B_{\perp} of 10 Gauss in the field-null region and a nominal toroidal field $B_T = 0.36\text{T}$ (60% of maximum toroidal field) at the plasma geometric center ($R_0 = 0.86\text{m}$). This value of the Lloyd parameter provides reliable plasma break-down in NSTX for all toroidal field values commonly used in the experiment, and the same specification is used for NSTX Upgrade ($R_{BD}=0.315\text{m}$) for a nominal toroidal field $B_T = 0.6\text{T}$ (again 60% of maximum toroidal field) at the Upgrade plasma geometric center ($R_0 = 0.93\text{m}$). To achieve this in the Upgrade, the available breakdown loop voltage is increased from 2.9 to 4.7V which requires an increase in the OH power supply voltage from 2.7kV to 4.1kV.

The ohmic flux required for plasma current ramp-up is a function of the plasma resistance which is a function of plasma temperature and Z_{eff} , and is therefore a function of auxiliary heating and current drive and confinement scenario (L-mode vs. H-mode). An early H-mode transition [35, 36] and NBI heating during the current ramp-up is commonly used on NSTX to minimize OH flux consumption to maximize the current flat-top duration.

Given the difficulty of accurately modeling the flux consumption required for break-down and ramp-up, Figure 3 shows the flux used to achieve a given flat-top plasma current for usage in extrapolating to NSTX Upgrade. As shown in Figure 3a, the total break-down plus ramp-up flux consumption extrapolates to 0.73Wb for NSTX shapes, which corresponds to 0.8Wb for NSTX Upgrade plasmas with larger major radius. As shown in Figure 3b, the major-radius-normalized total poloidal flux consumption (Ejima-Wesley coefficient [37, 38]) extrapolates to 0.3-0.35 which is approximately 60% of the ohmic plasma value in NSTX [39] for current ramp-rates near 5MA/s. Thus, including the breakdown+ramp-up flux required (0.8Wb) in addition to the current flat-top flux (1.3Wb), the total OH flux required increases by nearly a factor of 3 to 2.1Wb.

Finally, the ability to access normalized and toroidal beta values in NSTX-U comparable to those achieved in NSTX is also important for assessing the stability and transport as a function of beta and ν^* at reduced ν^* . For the ST confinement scaling, access to high temperature and beta is achievable with heating power comparable to that in NSTX, but for ITER H-mode scaling, substantially more power (factor of 2-3 times higher) is required to achieve similar beta values at similar safety factor q^* (see middle yellow and red columns in Table 1).

2.1.3. Center-stack Requirements and Design To summarize the combination of requirements above, the Upgraded NSTX device should: double B_T at $R=0.93\text{m}$ from 0.5T to 1T and increase the TF flat-top duration to 6-7s, double I_P from 1MA to 2MA and provide a 5s flat-top at full current, double the neutral beam injection (NBI) heating power from $P_{NBI} = 5\text{MW}$ to 10MW and sustain it for 5s, and nearly triple the OH flux from 0.75Wb to 2.1Wb. Representative waveforms for the NSTX and NSTX Upgrade currents are shown in Figure 4 and illustrate the substantial increase in device performance to be achieved with the Upgrade.

An important feature of the NSTX device design is the ability to remove the center-stack (CS) independent of the vacuum vessel and the external PF and TF magnets. Thus, Upgrade performance requirements can potentially be met by replacing the present CS with a new larger CS thereby providing more cross-sectional area and conductor to carry the TF current and also providing increased OH flux. The increased size of the new CS is shown graphically in Figure 5a by the red outline overdrawn on the present CS. Figure 5b shows the doubling of the TF conductor diameter which enables the doubling of TF current with 5 times longer pulses. The OH coil diameter also nearly doubles in the new CS, but the number of OH turns is decreased by 20% to increase the conductor cross-section and cooling hole diameter to enable inter-shot cool-down times of 15 minutes or less. As shown in Figure 5c, this larger CS incorporates the larger TF and OH while also including three upper and lower divertor PF coils PF1A,B,C (compared to two/one PF coils in the lower/upper divertor of NSTX) and also providing an insulating break for biasing the CS casing relative to the vessel for Coaxial Helicity Injection (CHI) current start-up. This larger outer diameter (OD) CS increases the minimum aspect ratio of fully limited plasmas from $A = 1.3$ to 1.5. As a result, diverted plasmas will typically have $A \geq 1.6$. While this aspect ratio is larger than the present NSTX, it is comparable to the optimal aspect ratio identified in ST-FNSF [3, 4], ST Pilot Plant [40], and ARIES-ST reactor studies [41].

2.1.4. Poloidal Field Requirements To enable engineering design of the upgrade, systematic free-boundary equilibrium calculations have been performed to determine the Upgrade poloidal field requirements. The design range spans aspect ratio $A = 1.6$ to 1.9, internal inductance $l_i = 0.4$ to 1.1, elongation $\kappa = 2.1$ to 2.9, triangularity $\delta = 0.2$ to 0.7, squareness $\zeta = -0.15$ to 0.12, magnetic balance $\delta_{Rsep} = -1.5$ to 0cm, normalized pressure $\beta_N = 1, 5,$ and 8, and OH solenoid current = 0 and $\pm 24\text{kA}$ (i.e. the power supply limits) to determine the divertor poloidal field (PF) needed for cancellation of

OH leakage flux. Figure 6 shows the 32 plasma boundaries of free-boundary equilibria used for assessing the PF coil current requirements for 2MA NSTX Upgrade plasmas. Each boundary shown is actually a plot of three plasma boundaries for each state of the OH coil current described above, and this set of 96 equilibria provides the set of configurations used for the detailed engineering design of the Upgrade. The PF coil currents for each configuration are shown in Figure 7 for 2MA plasmas with $\beta_N = 5$, and the PF coil locations and sizes and the minimum and maximum currents as a function of β_N are shown in Figure 8. As is evident from Figure 8, the most substantial changes in coil current for varied β_N are for the primary vertical field coil (PF5) and the inner-most divertor coil (PF1A).

2.1.5. Structural Enhancements In addition to accounting for variation in the plasma shape, the PF coil current requirements have also been assessed as a function of plasma current profile (internal inductance) and normalized beta for 2MA, 1T plasmas. The plasma inductance and beta primarily influence the required vertical field (PF5) coil current, and as shown in Figure 9, increased inductance and beta both increase the required vertical field. The Upgrade power supply system [42] is designed to increase the maximum PF5 current by 50% from 20kA to 30kA nominal maximum operating current. This enhancement will enable 2MA equilibria with β_N up to 5 at $l_i = 1$ and β_N up to 8 at $l_i = 0.6$, and this increased vertical field capability supports all scenarios used for the Upgrade design.

Doubling the TF and plasma current increases the forces on the coil supports and vacuum vessel up to a factor of 4, and substantial analysis and design has been performed to provide structural reinforcement against the increased loads. The NSTX Upgrade OH and PF coil turns-count and minimum and maximum currents used for the electromagnetic forces and structural analysis are summarized in Table 2. It should be noted that the PF2 and PF4 power supplies are nominally unipolar in the present NSTX and in the NSTX Upgrade design but can be upgraded to bipolar operation. As shown in Figure 10, the structural modifications include a new flexible umbrella upper lid to allow OH/TF vertical thermal expansion while transferring torsional loads of the CS to the outer vessel, new TF support rings and clevises to transfer torsional loads on the TF coils to the vacuum vessel, new and upgraded vertical field coil (PF4 and 5) separator struts to take increased inter-coil forces, and a new pedestal on which the CS is supported.

Another important design enhancement is the relocation of the OH coil current

leads from the top to the bottom of the centerstack to eliminate the stress on the leads arising from the vertical thermal expansion of the OH coil. Further, the OH coil lead area has been redesigned to utilize a coaxial current feed (shown in Figure 11) to minimize the non-axisymmetric fields from, and forces on, the OH coil which play a significant role in generating the $n=1$ error field in the present NSTX [27].

2.2. 2nd Neutral Beam Injector

2.2.1. Design Considerations Beyond the new CS and ex-vessel structural enhancements, a 2nd neutral beam from TFTR has been chosen to provide the factor of 2 increase in auxiliary heating and current drive power for NSTX Upgrade, as this is presently the most mature and capable technology applicable to ST plasma parameters. The performance parameters of the NSTX neutral beams [43] are provided in Figure 12 for reference. Of particular relevance is the decrease in achievable NBI pulse duration (set primarily by the thermal limits of the ion dumps) from 5s to 1.6s as the beamline power is increased 50% from 5MW to 7.5MW. This decrease highlights the importance of the 2nd NBI for providing sufficient heating power for the pulse-lengths expected in the Upgrade. If plasma scenarios with pulse-lengths substantially longer than 5s become accessible in NSTX Upgrade, additional NBI pulse-length enhancements may be possible by using "high-hat" ion dumps with two stacked plates (still inertially cooled) to spread the dumped beam ion footprint as originally proposed for the TPX NBI upgrade [44].

The 2nd NBI of NSTX Upgrade not only serves to increase the auxiliary heating power to access reduced ν^* , but also has increased tangency radius of injection R_{tan} . As shown in Figure 13a, increased R_{tan} substantially increases the current drive efficiency for non-inductive current ramp-up and sustainment. Achieving this increased tangency radius of injection requires a significant modification to the NSTX vacuum vessel with the cutting of a large opening in the vessel wall for the installation of a new NBI port cap as shown in Figure 13b. The injection radius of the present NSTX NBI has been left unchanged due to space constraints in the NSTX test cell.

The installation of the 2nd NBI also requires substantial floor space in the NSTX test cell, and a major task of the NSTX upgrade outage involves removing and relocating several diagnostics and associated racks to make room for the 2nd NBI. As shown in Figure 14, once the 2nd NBI is installed next to the present NBI, most of the available floor space within the test cell will be occupied by NSTX Upgrade and NBI systems. It should also be noted that the 2nd NBI to be used on NSTX Upgrade was used during the D-T experiments on TFTR and was contaminated with tritium. The decontamination

of this beam line was successfully completed in 2010 in preparation for usage on NSTX Upgrade, and reassembly of the 2nd NBI was initiated in 2011.

2.2.2. Non-inductive Current Sustainment A critical element of ST research in support of steady-state operation is to increase the 65-70% non-inductive fraction sustained in NSTX [45, 36, 46] to full non-inductive sustainment. Future ST-FNSF facilities are projected to rely heavily on NBI current drive (NBICD) to drive as much as 50% of the plasma current with the remainder provided by bootstrap current. Reduced collisionality in NSTX Upgrade will help increase the NBI current drive efficiency to increase the non-inductive fraction, but additional current drive is still required.

TRANSP [47] simulations indicate that more tangential NBI can increase NBICD efficiency by up to a factor of two - from $I_{NBICD}/P_{INJ} = 30\text{-}40\text{kA}/\text{MW}$ for the innermost $R_{tan}=50\text{cm}$ to up $70\text{-}80\text{kA}/\text{MW}$ for $R_{tan}=1.1\text{-}1.3\text{m}$, i.e. outboard of the magnetic axis (see Figure 15a). Further, for current profile control, variation of the NBICD deposition profile is needed. As shown in Figure 15a, the NBICD deposition profile depends only weakly on R_{tan} for the present NBI ($R_{tan} = 50, 60, 70\text{cm}$). In contrast, for the more tangential injection of the 2nd NBI in the Upgrade, $R_{tan} = 110, 120, 130\text{cm}$ can vary the injected NBICD parallel current density from centrally peaked to peaked off-axis. As shown in Figure 15b, using only the existing NBI with the CS upgrade, full-power NBI (7.5MW) + 4MW HHFW heating is needed to support 100% non-inductive operation, and the only means of q control is q_{min} variation through the plasma density (i.e. CD efficiency). Further, such scenarios require $H_{98}=1.2\text{-}1.4$ and would be limited to 1.6s duration by NBI ion dump operating limits as described above.

$H_{98}=1.3\text{-}1.4$ has been obtained transiently in NSTX, but sustaining $H_{98}=1.15\text{-}1.2$ is only now beginning to be achieved with Li conditioning [48] in ELM-free conditions in NSTX with a goal of extending this enhanced confinement to small-ELM regimes. With the addition of the 2nd NBI of the Upgrade, Figure 15c shows that higher NBI power (10MW vs. 7.5MW) can reduce the required confinement to $H_{98}=1.2$ for 100% non-inductive scenarios and also enables control of q_{min} with $\Delta q_{min} = 0.6$ by varying the NBI source mix at fixed density. Further, scenarios with $n_e/n_{Greenwald} = 0.7\text{-}1$ exist with q_{min} varying from 1 to above 2 with important implications for stability and transport research. All of the above scenarios operate above the $n=1$ no-wall stability limit and require stabilization of the resistive wall mode as is common for advanced scenarios on NSTX [25].

TRANSP calculations have also been carried out for 100% non-inductive current

drive using all 6 NBI sources at 1MA and 1T and by optimizing the outer gap to optimize the current drive profile. As shown in Figure 16a, 100% non-inductive current drive (indicated by the white line) is possible for a wide range of normalized density values with confinement multiplier $H_{98} = 1-1.05$. As shown in Figure 16b, q_{min} can be varied from values near 1 (indicated by the white line) to above 3 by varying the normalized density. Further, the q_{min} values can be increased well above 2 by operating at high normalized density with important implications for RWM stability and for avoiding $m/n = 2/1$ neoclassical tearing modes.

As shown in Figures 15 and 16, the electron density is a strong determinant of the expected NBI current drive efficiency, the non-inductive current fraction, and the expected value of minimum q. Thus, density control will be important for optimizing and controlling high non-inductive current-drive fraction scenarios (and other scenarios) in NSTX. Lithium coatings of the internal PFCs have been shown to pump hydrogenic species, improve confinement, and suppress ELMs in NSTX plasmas [49, 50]. Recently, control of the deuterium ion inventory to equivalent Greenwald fraction (ignoring impurities) as low as 0.3 has been achieved and sustained for up to 1.4s (limited by magnet heating) using Li coatings in NSTX. However, with strong lithiumization and in the absence of ELMs, carbon impurity accumulation can occur which increases the total (D^+ and C^{6+}) $Z_{eff} \leq 4$ corresponding to a Greenwald fraction of up to 0.8.

The combination of lithium coatings with ELMs triggered by externally applied $n=3$ non-axisymmetric field pulses [51] has successfully reduced the carbon accumulation and lowered the Z_{eff} to 3 or below corresponding to a minimum Greenwald fraction of 0.5-0.7. This range of achievable minimum Greenwald fraction is acceptable for optimizing the NBI current drive of NSTX Upgrade scenarios for pulse durations of perhaps 2-3s, but it is unclear if lithiumization combined with triggered ELMs will extrapolate to 5s pulses and higher heating powers of NSTX Upgrade. A liquid lithium divertor (LLD) [52, 53, 54, 55] is being tested in NSTX with a goal of assessing the ability of thicker layers of liquid lithium to extend the deuterium pumping duration relative to thin layers of solid lithium, and conceptual designs for divertor cryo-pumping systems will also be pursued for NSTX Upgrade. Such divertor particle pumping systems are not presently included in the scope of the NSTX Upgrade Project and would therefore likely be implemented following completion and initial usage of the new centerstack and second NBI.

2.2.3. *Non-inductive Current Formation and Ramp-up* To achieve low aspect ratio and small device size, future ST-FNSF facilities are anticipated to operate without a central solenoid, making non-inductive ramp-up (with reliance on NBI heating and CD) a critical element of ST research. Present NSTX research is pursuing non-inductive formation of plasma current using Coaxial Helicity Injection (CHI) [56] to form a closed-flux plasma of 0.2-0.3MA to be heated and sustained by high-harmonic fast-waves in a high bootstrap-current-fraction H-mode plasma. A major research goal of NSTX Upgrade is to assess whether plasmas formed with helicity injection and heated with ICRF and/or ECH/EBW can form a suitable target for current ramp-up using NBI heating and current drive.

CHI on NSTX is implemented by injecting current from an external circuit through a plasma arc formed along a combined poloidal and toroidal magnetic field that connects the lower inner and outer divertor plates. NSTX uses the lower divertor plates as the injector electrodes with the upper divertor plates acting (and referred to) as the absorber. At sufficiently high poloidal CHI injector current, the plasma current self-force accelerates the plasma away from the injector region into the vacuum chamber and toward the absorber region.

Figure 17a shows the rapid growth of the CHI plasma emerging from the lower divertor and filling the NSTX vacuum chamber in less than 3ms. As shown in Figure 17b, CHI has been successfully coupled to high-confinement inductively-driven plasmas [57, 58] with an early current savings of 150-200kA relative to OH-only start-up. As shown in Figure 17c, this corresponds to plasma poloidal flux formation by CHI of 50mWb. The plasmas compared in Figure 17 are chosen to have a similar shape and l_i value and evolution to illustrate the current and flux savings from CHI.

The initial poloidal field connecting the inner and outer divertor plates in the injector region is produced using the lower divertor coils as shown in Figure 18a. The "bubble burst" current threshold to inject a given amount of injector flux (poloidal flux) is given by the relation [56]:

$$I_{inj} = 2\psi_{inj}^2 / (\mu_0^2 d^2 I_{TF}) \quad (1)$$

Here ψ_{inj} is the poloidal flux at the injector insulating gap, I_{TF} is the total current in the toroidal field coil, and d is the width of injector flux footprint on the electrodes. It can also be shown that the toroidal current generated for a given amount of injector flux is given by the ratio of the toroidal flux enclosed by the ST limiter boundary Φ_{wall}

to the injector poloidal flux:

$$I_P \leq I_{inj} \Phi_{wall} / \psi_{inj} \quad (2)$$

Recent simulations with the TSC code [59] have shown reasonable agreement with these relations and the potential for substantial current generation in NSTX-U [60]. The reason for this can be seen in Figure 18a, which shows the location of the injector coil in relation to the CHI injector gap across which the voltage is applied. This improved current generation potential in NSTX-U is due to the improved location of the CHI injector flux coil (lower PF1C coil), which is positioned much closer to the CHI insulating gap. As shown in Figure 18a, the injector coil in NSTX is farther away from the insulating gap, resulting in a 2.5 times smaller flux generated by this coil that connects the inner and outer divertor plates. Quantitatively, the available injector flux in NSTX-U is projected to be approximately 200 mWb compared to less than 80 mWb in NSTX.

In addition to the improved positioning of the lower divertor PF coils in NSTX-U for CHI, Figure 18b shows that the location of the absorber coil (upper PF1C coil) is better positioned in NSTX-U. This coil is used to generate a buffer flux to keep the expanding CHI discharge from contacting the upper absorber gap, as such a condition (known as an absorber arc) can short-circuit the insulating gap and cause the injected current to flow through this gap instead of through the main plasma. The closer positioning of the PF1C coil to the absorber gap enables the flux generated by this coil to be more efficiently utilized to suppress absorber arcs. Importantly, the kA-turn capability of the absorber coil in NSTX-U is three times that in NSTX (318 kA-turn versus 100 kA-turn in NSTX) and the current slew rate is also substantially higher (40 kA-turn/ms in NSTX-U versus 5 kA-turns/ms in NSTX). The faster slew rates are needed to rapidly turn off the lower divertor PF coils after the CHI plasma formation process is complete and to track the rapid upward motion of the higher-current CHI plasma expected in NSTX-U. Overall, CHI current formation scales favorably with the available injector flux and the enclosed toroidal flux, and CHI is projected to be capable of generating 300-600kA of closed-flux current in NSTX Upgrade by operating at 1T based on scaling the results of Figure 17 and TSC simulations [60].

Moving to the consideration of non-inductive current ramp-up, a very important benefit of more tangential NBI is the ability to heat and drive current in low current target plasmas. As shown in Figure 19a for low $I_p=0.4\text{MA}$ target plasmas, the NBI power losses (presently dominated by bad-orbit losses) are predicted to be reduced by up to a factor of 3 with the increased R_{tan} of the 2nd NBI of the Upgrade. As shown in

Figure 19b, this translates into a factor of 3 increase in CD efficiency of up to 60kA/MW for the 2nd NBI. As is evident from Figure 19b, the tangency radii of the 2nd NBI are close to the optimal values (by design) for maximizing the NBICD at low plasma current. As shown in Figure 19c-d, TSC simulations indicate this 400-450kA of NBICD is sufficient to non-inductively over-drive a 0.4MA target plasma to a 0.8-0.9MA flat-top current. Thus, by operating at 1T and combining CHI current formation of 300-600kA to NBI current ramp-up with the 2nd NBI, NSTX Upgrade is very well equipped to study non-inductive current formation and ramp-up as needed for an ST-FNSF.

2.3. Disruption Forces

Just as the equilibrium electromagnetic forces on the structure will increase by up to a factor of 4 in NSTX Upgrade, the forces during plasma disruptions are expected to increase by a similar factor. The projections for NSTX Upgrade rely heavily on the previous characterization of vertical displacement events (VDEs) and plasma current quenches (CQs) from NSTX [61]. Based on NSTX data and scalings, 3D electromagnetic models of the vacuum vessel and passive conducting structures of NSTX have been utilized to predict the induced currents, fields, and forces for 2MA, 1T plasma disruptions in NSTX Upgrade [62]. One concern is the stress applied to the passive plates, and the possibility of radial plate displacements and deformation caused by Lorentz forces resulting from toroidal currents circulating in the plate crossed with the (coil plus plasma) poloidal magnetic field. Since the passive plates play an important role in vertical stability and resistive wall mode stabilization in NSTX and NSTX Upgrade, using higher strength but more resistive plate material (such as stainless steel) is likely not an acceptable option.

Using the simplified plasma vertical displacement model for NSTX Upgrade [62], Figure 20a shows the lower passive plate current density induced by the downward vertical drift of a 2MA plasma with a drift duration of 10ms. Simulations using Opera and ANSYS analysis software find that VDE drift durations in this range maximize the induced circulating currents and radial forces on the passive plates. Figure 20b shows that the peak plate deflection is approximately 1mm as indicated by the orange and red contours near the top and bottom of the passive plate at the plate toroidal mid-point between the plate supports. The corresponding peak membrane plus bending stress is 60MPa which is a factor of 3 below the yield stress. This stress level found at the mid-point between the plate supports is acceptable for NSTX Upgrade. However, the stresses near the bolt heads attaching the plates to the supports are above allowable

limits, and at a minimum, enhancements such as higher-strength bolts and/or larger bolt-head slots and washers will be required to withstand the increased disruption loads of NSTX Upgrade.

If plate attachment enhancements are found to be insufficient or infeasible, or if it is desired in the future to increase the maximum plasma current to above 2MA in NSTX Upgrade, one possible means of reducing the peak stress and radial displacement during disruptions is to use thicker passive plates. For fixed applied load, the plate displacement scales as the inverse of the thickness cubed, so doubling the CuCrZr plate thickness from 0.5 inches to 1 inch could substantially reduce the plate deflection under disruption loads. However, the increased conductance of the thicker plate could increase the induced current, which could reduce the effectiveness of thicker plates, and would also increase the penetration time of fields normal to the passive plates.

In addition to the 3D modeling, the LRDFIT [63] axisymmetric-equivalent circuit model of the coils and passive conducting regions has been developed, benchmarked, and extensively used for NSTX and is used here to assess the impact of thicker plates. Figure 21 shows the LRDFIT-reconstructed plasma and plate current evolution for a representative VDE disruption in NSTX. As seen in Figure 21a for a downward VDE, the chosen plasma drifts from nearly vertically centered to being limited on the lower divertor plate in 5-10ms which is comparable to the drift duration of the simulated case of Figure 20. As shown in Figure 21b, during this drift phase, the plasma cross-section is reduced while the plasma current is maintained. As is evident from Figures 21c and d, the net toroidal plate current induced by the plasma motion is negative as the plate currents act to oppose the downward vertical plasma motion. Then, as the current quench occurs over the subsequent 2-3ms, the net toroidal plate current induced by the quench is reversed and becomes positive in response to the loss of positive plasma current and poloidal magnetic energy.

An important aspect of the NSTX passive structure design is that the stainless steel supports connecting the plates to the vessel wall are several orders of magnitude more resistive than the CuCrZr passive plates, and therefore the net toroidal current is effectively unchanged by increasing the plate thickness. For this reason, Figures 21c and d only plot the net toroidal current for the present 0.5in thick passive plates, since the currents are nearly identical for the two plate thicknesses. In contrast, the circulating current magnitudes do increase with plate thickness since the plate resistance is reduced. The maximum circulating currents in Figure 21c and d are approximately 1.5 times higher for the 1.0 inch thick plates versus the present 0.5 inch plates. Also, after the

end of the CQ, the circulating currents in the thicker plates are approximately a factor of 2 times higher and decay away more slowly due to the lower plate resistance and longer L/R time. It is noted however that these increased currents occur after the CQ, so there is little impact of these currents on the plasma current flat-top phase. Further, modeling of the plasma current ramp-up finds that these currents are sufficiently small that they would not significantly impact normal plasma operations.

In the analysis described above and shown in Figures 21 and 22, the circulating current is defined as $I_{circ} = \frac{1}{2} \sum_j |I_j - I_{avg}|$ where I_j is the toroidal current in conducting element i of a conducting region, each conducting element cross-sectional area is identical in a given region, and I_{avg} is the average value of I_j . Thus, if the current density in a region is constant, I_j will be constant, and $I_{circ} = 0$. Correspondingly, if the net toroidal current is zero, $I_{avg} = 0$, and I_{circ} is equivalent to the total positive toroidal current flowing in the region.

To further analyze the distribution of current in the passive plates, Figure 22 plots the plate toroidal current density for the shot in Figure 21 at $t=403\text{ms}$ at the time of peak net toroidal current and Lorentz pressure which is just after the time of peak circulating current magnitude. As shown in Figures 22a and b the maximum current density occurs near the top end of each plate where the net toroidal and circulating components are additive in the positive (co-plasma current) direction, while the negative current density occurs on the bottom of each plate with a magnitude typically less than the peak positive value. At this time during the disruption evolution, Figures 22a and b show that some of the negative current density is carried on the back each plate, and similar skin effects are observed in the Opera electromagnetic simulations of Figure 20a. These results highlight the importance of using models that include finite conductor thickness to accurately assess VDE induced currents in passive conducting structures. Further, Figures 22b shows that the peak positive current density of the thicker plate is 15-22% lower than for the thinner plate. This reduction likely contributes to the peak circulating current magnitude in the thicker plate being less than a factor of two higher than in the thinner plate.

The peak plate toroidal current density during the disruption evolution of Figure 21 is $\approx 33\text{MA}/\text{m}^2$ which scaled (by a factor of 1.6) to the worst-case net toroidal current for 0.7MA NSTX plasmas [61] and then scaled (by a factor of 3) to 2MA plasmas projects to $160\text{MA}/\text{m}^2$ in NSTX Upgrade. This value is in good quantitative agreement with 3D predictions of the peak plate current density of $120\text{-}160\text{MA}/\text{m}^2$ for the simulated plasma vertical drift scenario shown in Figure 20a. Overall, this analysis indicates that

a doubling of plate thickness would result in an increase in plate circulating current by a factor of 1.5-2 and result in an estimated net 4-5 fold reduction in plate displacement, i.e. plate displacement comparable to present NSTX values and therefore capable of handling 2MA disruptions with an expectation of no plate damage over the lifetime of the Upgrade.

2.4. Resistive Wall Mode Stability

The ability to withstand disruptions of the highest performance plasmas of the Upgrade maintains a vital capability, namely the ability to access and study high beta plasmas at the highest possible plasma temperature and lowest collisionality without risking machine integrity. As described in Section 2.1, several structure enhancements are included of the Upgrade design to support high β operation at full field and current. As described in Section 2.2.1, the 2nd NBI will introduce another large vessel penetration as shown in Figure 13b. Since this penetration will no longer have a metal port cover, the area of the conducting wall will be reduced, and this could adversely impact resistive wall mode (RWM) stability [25] during operation above the no-wall stability limit. However, in NSTX, by design, the CuCrZr passive conducting plates provide much of the stabilization of the RWM. To assess the impact of the 2nd NBI port, the VALEN code [64] has been utilized to analyze n=1 RWM stability for NSTX Upgrade. Figure 23a shows the VALEN model for the passive conducting structure of the Upgrade including both the present and 2nd NBI ports. Figure 23b shows the calculated n=1 RWM growth rates as a function of β_N and number of NBI ports for a representative 2MA equilibrium (equilibrium "R" in Figure 6) with $A=1.7$, $\kappa=2.6$, $\delta = 0.6$, $l_i=0.6$, and $q_{min}=1.9$. As is evident from Figure 23b, the addition of the 2nd NBI results in only a small β_N decrement of $\Delta\beta_N = -0.07$ from 5.79 to 5.72 indicating that the 2nd NBI port will have negligible impact on RWM stability limits in NSTX Upgrade.

The n=1 kink with-wall stability limit shown in Figure 23b is for an equilibrium using scaled pressure and parallel current density profiles taken from an MHD-stable NSTX experimental plasma (shot 1163136) operating at $\beta_N = 5.5$ above the no-wall limit and near the with-wall limit [45]. In using these profiles from NSTX for NSTX Upgrade free-boundary equilibrium calculations, the profiles have not been further optimized to increase stability limits. It should be noted that the NSTX Upgrade with-wall limit shown in Figure 23b extrapolates to $\beta_N \approx 5.9$ in the absence of NBI port penetrations. This β_N value is approximately 15% lower than computed in the original NSTX RWM control system design using VALEN [65] (also ignoring port penetrations) for lower

aspect ratio NSTX plasmas. Previous numerical studies have shown that both no-wall and with-wall stability limits are projected to decrease 10-20% as the aspect ratio is increased from $A=1.45$ to 1.7 [66, 67]. Thus, the decrease in kink stability limits from NSTX to NSTX Upgrade can be attributed in large part to increased aspect ratio.

2.5. Divertor Power Handling

While the compactness of the ST is beneficial for achieving high neutron wall loading for FNS, the ST divertor heat fluxes can also be high and challenge PFC power handling capabilities. The width of the heat-flux profile in the SOL is a critical parameter in projecting the peak divertor heat flux, since the peak heat flux varies inversely with this width. Multi-machine databases and scalings exhibit a wide variation in predicted outboard midplane SOL heat flux width λ_q and this variation represents a substantial uncertainty in projecting to future devices including ITER [68]. Recent dedicated multi-machine studies in the U.S. [69, 70, 71] have explored the λ_q scaling further and find a strong inverse dependence on plasma current but a weak dependence on magnetic field and power into the SOL. Using this mid-plane heat-flux width parameter, the peak heat flux to the divertor can be expressed as:

$$Q_{out}^{peak} = \frac{P_{heat}^{SOL}(1 - f_{rad})f_{div} \sin(\theta_{plate})}{2\pi R_{strike} f_{exp} \lambda_q} \quad (3)$$

where P_{heat}^{SOL} is the heating power to the SOL in the absence of radiative losses, f_{rad} is the assumed fraction of radiation, f_{div} is the fraction of SOL power to divertor leg in question, θ_{plate} is the poloidal angle of inclination between the divertor plate and divertor magnetic field lines, R_{strike} is the major radius of the divertor strike-point, and f_{exp} is the poloidal flux expansion = $|\nabla\psi|_{midplane}/|\nabla\psi|_{strike}$.

Of particular importance for NSTX Upgrade are high current (2MA) plasmas which are projected to have SOL heat-flux widths as narrow as 3mm. As shown in Figure 24, the peak heat flux must be limited to $10\text{MW}/\text{m}^2$ to enable 5s operation with the inertially/radiatively cooled ATJ graphite PFCs planned for the Upgrade. Recent assessments of the divertor heat flux scaling in NSTX project to peak divertor heat fluxes over $20\text{MW}/\text{m}^2$ in the Upgrade even assuming high poloidal flux expansions of 30 [71]. As indicated in Figure 24, utilizing upper/lower power-splitting but not accounting for any radiation/detachment or strike-point sweeping, poloidal flux expansions of 60 are required to achieve peak heat-flux near $10\text{MW}/\text{m}^2$ for $P_{heat} = 12\text{MW}$ in 2MA plasmas.

Very high flux expansions of 40-60 have recently been demonstrated in NSTX utilizing a "snowflake" [72] divertor as shown in Figure 25a. In order to support this

and other future high-flux-expansion divertors such as the “Super-X” [73] (possible with additional in-vessel PF coils not part of the present Upgrade), additional divertor PF coils have been incorporated into the Upgrade CS design as shown in Figure 5c. In particular, a third divertor PF coil (PF1C) will be added to the CS as shown in Figure 25b to support the snowflake and to improve control of flux expansion and strike-point location generally. Importantly, the snowflake divertor has recently demonstrated large (factor of 3 or more) reductions in peak heat flux as shown in Figure 26, and also up to a 50% reduction in carbon impurity production [74]. Increased divertor radiation and partial detachment is another possible means to reduce the peak divertor heat load while maintaining high core plasma performance as previously shown in NSTX [75]. Overall, the snowflake divertor projects favorably to mitigating high divertor heat fluxes in NSTX Upgrade and for supporting flat-top durations up to 5s at a plasma current of 2MA. Larger normalized strike-point radius (R_{strike}/R_0) and the effects of very large parallel connection length will also be extensively investigated in MAST Upgrade which is designed specifically to incorporate a cryo-pumped “Super-X” divertor [73]. NSTX Upgrade (and MAST Upgrade) with increased current, field, and power will not only substantially extend and improve the understanding of the scaling of SOL heat flux width with plasma parameters, but will also contribute to the development of novel means of mitigating high heat flux for FNSF and for Demo.

3. Summary

Scoping studies for a range of ST energy confinement assumptions have been performed for NSTX Upgrade with a goal of determining the performance requirements to achieve a factor of 3-6 reduction in collisionality, support tests of 100% non-inductive current ramp-up and sustainment, and assess confinement, stability, and heat-flux scaling and mitigation at increased magnetic field and plasma current while also providing sufficient flat-top duration for profile equilibration. The scoping studies indicate that a factor of two increase in plasma current, toroidal field, and NBI auxiliary heating power, a factor of 3 increase in ohmic solenoid flux, and a quintupling of the flat-top duration are sufficient to achieve the Upgrade goals. These performance objectives can be achieved with the combination of a new center-stack and a 2nd more tangentially injecting NBI.

Systematic free-boundary equilibrium calculations have been performed to assess the poloidal field coil current requirements to support the higher plasma current and access to high beta, and substantial engineering analysis and design has been performed

for the structural reinforcements needed to handle the increased electromagnetic loads. In addition to the ex-vessel structural enhancements, the new CS incorporates numerous design improvements, including more robust flexible TF connections from the inner to outer TF legs, and a bottom-fed coaxial lead for the OH coil designed to substantially reduce the present NSTX $n=1$ error field induced by an OH-TF electromagnetic interaction.

The 2nd neutral beam injector included in the Upgrade is designed to inject much more tangentially than the present NBI, and this injection geometry is predicted to increase the NBI CD efficiency by up to a factor of 2 enabling 100% non-inductive current drive at the 1MA level and control of the core safety factor profile. Importantly, the 2nd NBI is also computed to have 2 times higher fast-ion confinement (due to reduced bad orbit loss) at low plasma current as needed for non-inductive ramp-up studies. Also in support of non-inductive current ramp-up studies, the new CS incorporates additional poloidal field coils in the divertor to increase Coaxial Helicity Injection (CHI) injector flux by a factor of 2.5, increase the absorber coil current a factor of 3, and increase the absorber coil slew rate by a factor of 8. The higher TF and enhanced CS PF coil and CHI capability combined with the 2nd NBI are projected to be capable of non-inductive start-up of at least 300kA and ramp-up to the 0.8-1MA-level. The more tangential NBI requires a significant modification to the NSTX vacuum vessel through the addition of a radially offset port cap. Further, the 2nd NBI requires considerable test-cell floor space and relocation of numerous diagnostics and associated racks and equipment.

Just as the equilibrium electromagnetic forces are expected to increase by up to a factor of four, disruption loads are anticipated to increase by a similar factor. The disruption forces from induced currents in the passive conducting plates are sufficiently high that additional plate re-enforcements (particularly at the plate attachment points) or thicker plates may be required. If thicker plates are utilized, the plate circulating current (but not the net toroidal current) is predicted to increase due to decreased plate resistance. However, despite the increased plate circulating current, it is expected that the plate displacement/deformation could be significantly reduced by the increased passive plate thickness. With respect to the achievable beta in the Upgrade, the structural enhancements support operation at high β_N up to 8 at full current and field at low l_i . The addition of a 2nd NBI port and associated reduction in conducting wall area is computed to produce only a small reduction on the ideal-wall limit.

Finally, the divertor heat flux width is observed to scale inversely with plasma current in NSTX and could lead to very high heat fluxes in the NSTX Upgrade divertor

at maximum current and heating power. The high-flux-expansion "snowflake" divertor has demonstrated considerable heat flux reduction in NSTX, and the incorporation of additional PF coils in the new CS enables operation with upper and lower snowflake divertors. Up/down power splitting using upper and lower snowflake divertors is projected to reduce the peak divertor heat flux to $10\text{MW}/\text{m}^2$ and inertially maintain divertor tile temperature below sublimation damage limits for 5s pulses at full current and high heating power.

In summary, the new capabilities of the NSTX Upgrade are anticipated to greatly enhance ST research in support of assessing the ST as a potential Fusion Nuclear Science Facility (FNSF). The NSTX Upgrade project is presently scheduled to be completed in 2014.

Acknowledgments

This manuscript has been authored by Princeton University under Contract No. DE-AC02-09CH11466 with the U.S. Department of Energy. The publisher, by accepting the article for publication, acknowledges that the United States Government retains a non-exclusive, paid-up, irrevocable, world-wide license to publish or reproduce the published form of this manuscript, or allow others to do so, for United States Government purposes.

References

- [1] PENG, Y.-K. M. and STRICKLER, D. J., Nucl. Fus. **26** (1986) 769.
- [2] PENG, Y.-K. M., GALAMBOS, J. D., and SHIPE, P. C., Fus. Technol. **21** (1992) 1729.
- [3] PENG, Y.-K. M., FOGARTY, P. J., BURGESS, T. W., STRICKLER, D. J., NELSON, B. E., et al., Plasma Phys. and Contr. Fus. **47** (2005) B263.
- [4] PENG, Y.-K. M., BURGESS, T. W., CARROLL, A. J., NEUMEYER, C. L., CANIK, J. M., et al., Fusion Sci. Technol. **56** (2009) 957.
- [5] KAYE, S. M., ONO, M., PENG, Y.-K., BATCHELOR, D. B., CARTER, M. D., et al., Fus. Technol. **36** (1999) 16.
- [6] ONO, M., KAYE, S. M., PENG, Y.-K. M., BARNES, G., BLANCHARD, W., et al., Nucl. Fus. **40** (2000) 557.
- [7] KAYE, S. M., LEVINTON, F. M., STUTMAN, D., TRITZ, K., YUH, H., et al., Nucl. Fus. **47** (2007) 499.
- [8] VALOVIC, M., AKERS, R., CUNNINGHAM, G., GARZOTTI, L., LLOYD, B., et al., Nucl. Fus. **49** (2009) 075016.
- [9] VALOVIC, M., AKERS, R., DE BOCK, M., MCCONE, J., GARZOTTI, L., et al., Nucl. Fus. **51** (2011) 073045.
- [10] KAYE, S. M., BELL, R. E., GATES, D., LeBlanc, B. P., LEVINTON, F. M., et al., Phys. Rev. Lett. **98** (2007) 175002.
- [11] MAZZUCATO, E., SMITH, D. R., BELL, R. E., KAYE, S. M., HOSEA, J. C., et al., Phys. Rev. Lett. **101** (2008) 075001.
- [12] MAZZUCATO, E., BELL, R. E., ETHIER, S., HOSEA, J. C., KAYE, S. M., et al., Nucl. Fus. **49** (2009) 055001.
- [13] SMITH, D. R., KAYE, S. M., LEE, W., MAZZUCATO, E., PARK, H. K., et al., Phys. Rev. Lett. **102** (2009) 225005.
- [14] YUH, H. Y., KAYE, S. M., LEVINTON, F. M., MAZZUCATO, E., MIKKELSEN, D. R., et al., Phys. Rev. Lett. **106** (2011) 055003.
- [15] REN, Y., KAYE, S. M., MAZZUCATO, E., GUTTENFELDER, W., BELL, R. E., et al., Phys. Rev. Lett. **106** (2011) 165005.
- [16] STUTMAN, D., Delgado-Aparicio, L., GORELENKOV, N., FINKENTHAL, M., FREDRICKSON, E., et al., Phys. Rev. Lett. **102** (2009) 115002.
- [17] GORELENKOV, N. N., STUTMAN, D., TRITZ, K., BOOZER, A., Delgado-Aparicio, L., et al., Nucl. Fus. **50** (2010) 084012.
- [18] WONG, K. L., KAYE, S., MIKKELSEN, D. R., KROMMES, J. A., HILL, K., et al., Phys. Rev. Lett. **99** (2007) 135003.
- [19] WONG, K. L., KAYE, S., MIKKELSEN, D. R., KROMMES, J. A., HILL, K., et al., Phys. Plasmas **15** (2008) 056108.
- [20] SMITH, D. R., GUTTENFELDER, W., LeBlanc, B., and MIKKELSEN, D., Plasma Phys. and Contr. Fus. **53** (2011) 035013.
- [21] GUTTENFELDER, W., CANDY, J., KAYE, S. M., NEVINS, W. M., WANG, E., et al., Phys. Rev. Lett. **106** (2011) 155004.
- [22] HORTON, W., ZHU, P., HOANG, G. T., ANIEL, T., OTTAVIANI, M., et al., Phys. Plasmas **7**

- (2000) 1494.
- [23] ZHU, W., SABBAGH, S. A., BELL, R. E., BIALEK, J. M., BELL, M. G., et al., Phys. Rev. Lett. **96** (2006) 225002.
 - [24] PARK, J. K., BOOZER, A. H., and MENARD, J. E., Phys. Rev. Lett. **102** (2009) 065002.
 - [25] SABBAGH, S. A., BERKERY, J. W., BELL, R. E., BIALEK, J. M., GERHARDT, S. P., et al., Nucl. Fus. **50** (2010) 025020.
 - [26] BERKERY, J. W., SABBAGH, S. A., BETTI, R., BELL, R. E., GERHARDT, S. P., et al., Phys. Rev. Lett. **106** (2011) 075004.
 - [27] MENARD, J. E., BELL, R. E., GATES, D. A., GERHARDT, S. P., PARK, J.-K., et al., Nucl. Fus. **50** (2010) 045008.
 - [28] GERHARDT, S. P., MENARD, J. E., PARK, J.-K., BELL, R., GATES, D. A., et al., Plasma Phys. and Contr. Fus. **52** (2010) 104003.
 - [29] MAINGI, R., HUBBARD, A. E., MEYER, H., HUGHES, J. W., KIRK, A., et al., Nucl. Fus. **51** (2011) 063036.
 - [30] ITER Physics Expert Groups on Confinement and Transport and Confinement Modelling and Database and ITER Physics Basis Editors, Nucl. Fus. **39** (1999) 2175.
 - [31] DOYLE, E., HOULBERG, W., KAMADA, Y., MUKHOVATOV, V., OSBORNE, T., et al., Nucl. Fus. **47** (2007) S18.
 - [32] GREENWALD, M., TERRY, J. L., WOLFE, S. M., EJIMA, S., BELL, M. G., et al., Nucl. Fus. **28** (1988) 2199.
 - [33] GREENWALD, M., Plasma Phys. and Contr. Fus. **44** (2002) R27.
 - [34] LLOYD, B., JACKSON, G., TAYLOR, T., LAZARUS, E., LUCE, T., et al., Nucl. Fus. **31** (1991) 2031.
 - [35] MENARD, J. E., BELL, R. E., FREDRICKSON, E. D., GATES, D. A., KAYE, S. M., et al., Nucl. Fus. **45** (2005) 539.
 - [36] GATES, D. A., KESSEL, C., MENARD, J., TAYLOR, G., WILSON, J., et al., Nucl. Fus. **46** (2006) S22.
 - [37] EJIMA, S., CALLIS, R. W., LUXON, J. L., STAMBAUGH, R. D., TAYLOR, T. S., et al., Nucl. Fus. **22** (1982) 1313.
 - [38] WESLEY, J., BELJAKOV, V., BULMER, R., HOGAN, J., KAISER, T., et al., The ITER poloidal field system, in *Plasma Physics and Controlled Nuclear Fusion Research 1990*, volume 3 of *Thirteenth conference proceedings*, p. 421, Washington, DC, 1991, International Atomic Energy Association, Vienna.
 - [39] MENARD, J. E., LEBLANC, B. P., SABBAGH, S. A., BELL, M. G., BELL, R. E., et al., Nucl. Fus. **41** (2001) 1197.
 - [40] MENARD, J. E., BROMBERG, L., BROWN, T., BURGESS, T., DIX, D., et al., Nucl. Fus. **51** (2011) 103014.
 - [41] NAJMABADI, F. and The ARIES Team, Fus. Engin. and Design **65** (2003) 143.
 - [42] RAMAKRISHNAN, S., NEUMEYER, C., LAWSON, J., MOZULAY, R., BAKER, E., et al., Power system for NSTX Upgrade, 24th IEEE Symposium on Fusion Engineering, 2011, Chicago IL.
 - [43] STEVENSON, T., MCCORMACK, B., LOESSER, G. D., KALISH, M., RAMAKRISHNAN, S., et al., A neutral beam injector upgrade for NSTX, 2002, PPPL Report 3651.

- [44] DAHLGREN, F., WRIGHT, K., KAMPERSCHROER, J., GRISHAM, L., LONTAI, L., et al., TPX/TFTR neutral beam energy absorbers, in *Proceedings of the 15th IEEE/NPSS Symposium on Fusion Engineering*, volume 1, pp. 455–461, 1993.
- [45] MENARD, J. E., BELL, R. E., GATES, D. A., KAYE, S. M., LEBLANC, B. P., et al., *Phys. Rev. Lett.* **97** (2006) 095002.
- [46] GERHARDT, S. P., FREDRICKSON, E., GATES, D., KAYE, S., MENARD, J., et al., *Nucl. Fus.* **51** (2011) 033004.
- [47] GOLDSTON, R. J., MCCUNE, D. C., and TOWNER, H. H., *J. Comput. Phys.* **43** (1981) 61.
- [48] MAINGI, R., BELL, R. E., CANIK, J. M., GERHARDT, S. P., KAYE, S. M., et al., *Phys. Rev. Lett.* **25** (2010) 135004.
- [49] KUGEL, H. W., MANSFIELD, D., MAINGI, R., BELL, M. G., BELL, R. E., et al., *J. Nucl. Mater.* **390-391** (2009) 1000.
- [50] BELL, M. G., KUGEL, H. W., KAITA, R., ZAKHAROV, L. E., SCHNEIDER, H., et al., *Plasma Phys. and Contr. Fus.* **51** (2009) 124054.
- [51] CANIK, J. M., MAINGI, R., EVANS, T. E., GERHARDT, R. E. B. S. P., LEBLANC, B. P., et al., *Phys. Rev. Lett.* **104** (2010) 045001.
- [52] KUGEL, H. W., BELL, M., BERZAK, L., BROOKS, A., ELLIS, R., et al., *Fus. Engin. and Design* **84** (2009) 1125.
- [53] ELLIS, R., KAITA, R., KUGEL, H., PALUZZI, G., VIOLA, M., et al., Mechanical design of the NSTX liquid lithium divertor, 23rd IEEE/NPSS Symposium on Fusion Engineering, 2009, San Diego, CA.
- [54] NYGREN, R. E., HARJES, H. C., WAKELAND, P., ELLIS, R., KUGEL, H. W., et al., *Fus. Engin. and Design* **84** (2009) 1438.
- [55] ALLAIN, J. P. and BROOKS, J. N., *Nucl. Fus.* **51** (2011) 023002.
- [56] JARBOE, T. R., *Fus. Technol.* **15** (1989) 7.
- [57] RAMAN, R., MUELLER, D., NELSON, B. A., JARBOE, T. R., GERHARDT, S., et al., *Phys. Rev. Lett.* **104** (2010) 095003.
- [58] NELSON, B. A., JARBOE, T. R., MUELLER, D., RAMAN, R., BELL, M., et al., *Nucl. Fus.* **51** (2011) 063008.
- [59] JARDIN, S. C., POMPHREY, N., and DELUCIA, J., *J. Comput. Phys.* **66** (1986) 481.
- [60] RAMAN, R., JARDIN, S. C., MENARD, J., and JARBOE, T. R., *Nucl. Fus.* (2011), accepted for publication.
- [61] GERHARDT, S. P., MENARD, J. E., and the NSTX Team, *Nucl. Fus.* **49** (2009) 025005.
- [62] TITUS, P. H., AVASARALLA, S., BROOKS, A., and HATCHER, R., *Fus. Engin. and Design* (2011), in press.
- [63] MENARD, J. E., <http://w3.pppl.gov/jmenard/software/lrdfit/lrdfit-index.htm>.
- [64] BIALEK, J., BOOZER, A. H., MAUEL, M. E., and NAVRATIL, G. A., *Phys. Plasmas* **8** (2001) 2170.
- [65] SABBAGH, S. A., BIALEK, J. M., BELL, R. E., GLASSER, A. H., LEBLANC, B. P., et al., *Nucl. Fus.* **44** (2004) 560.
- [66] MENARD, J. E., JARDIN, S. C., KAYE, S. M., KESSEL, C. E., and MANICKAM, J., *Nucl. Fus.* **37** (1997) 595.
- [67] MENARD, J. E., BELL, M. G., BELL, R. E., GATES, D. A., KAYE, S. M., et al., *Phys. Plasmas*

- 11** (2004) 639.
- [68] LOARTE, A., LIPSCHULTZ, B., KUKUSHKIN, A., MATTHEWS, G., STANGEBY, P., et al., Nucl. Fus. **47** (2007) S203.
- [69] LABOMBARD, B., TERRY, J. L., HUGHES, J. W., BRUNNER, D., PAYNE, J., et al., Phys. Plasmas **18** (2011) 056104.
- [70] LASNIER, C. J., MAKOWSKI, M. A., BOEDO, J. A., ALLEN, S. L., BROOKS, N. H., et al., J. Nucl. Mater. (2011), in press.
- [71] GRAY, T. K., MAINGI, R., SOUKHANOVSII, V. A., SURANY, J. E., AHN, J.-W., et al., J. Nucl. Mater. (2011), in press.
- [72] RYUTOV, D. D., Phys. Plasmas **14** (2007) 064502.
- [73] VALANJU, P. M., KOTSCHENREUTHER, M., MAHAJAN, S. M., and CANIK, J., Phys. Plasmas **16** (2009) 056110.
- [74] SOUKHANOVSII, V. A., AHN, J.-W., BELL, R. E., GATES, D. A., GERHARDT, S., et al., Nucl. Fus. **51** (2011) 012001.
- [75] SOUKHANOVSII, V. A., MAINGI, R., GATES, D. A., MENARD, J. E., RAMAN, S. F. P. R., et al., Nucl. Fus. **49** (2009) 095025.

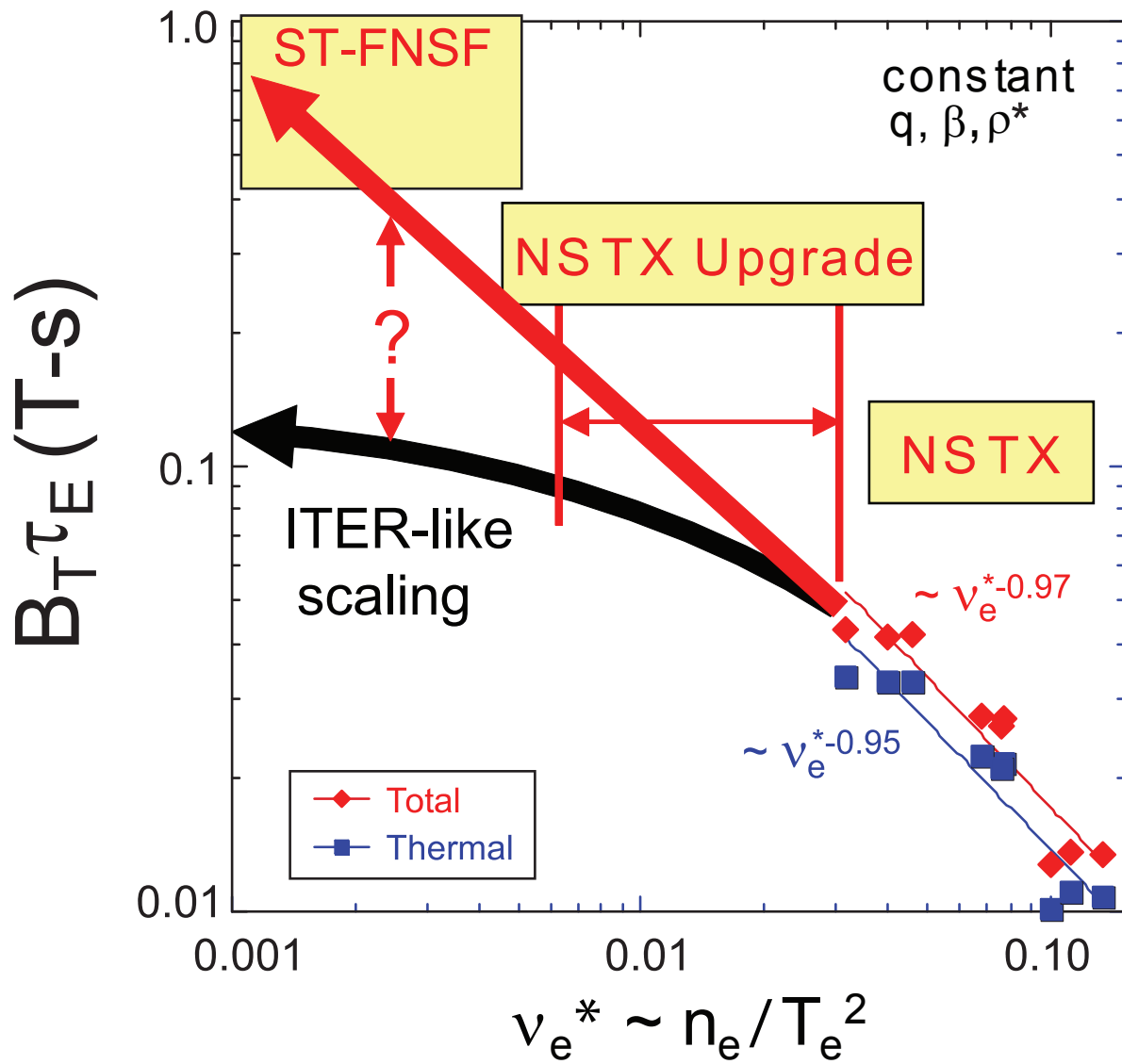


Figure 1. Product of toroidal field (B_T) and energy confinement time (τ_E) versus ν_e^* for NSTX and projections for NSTX Upgrade and ST-FNSF for ITER H-mode and ST confinement scalings.

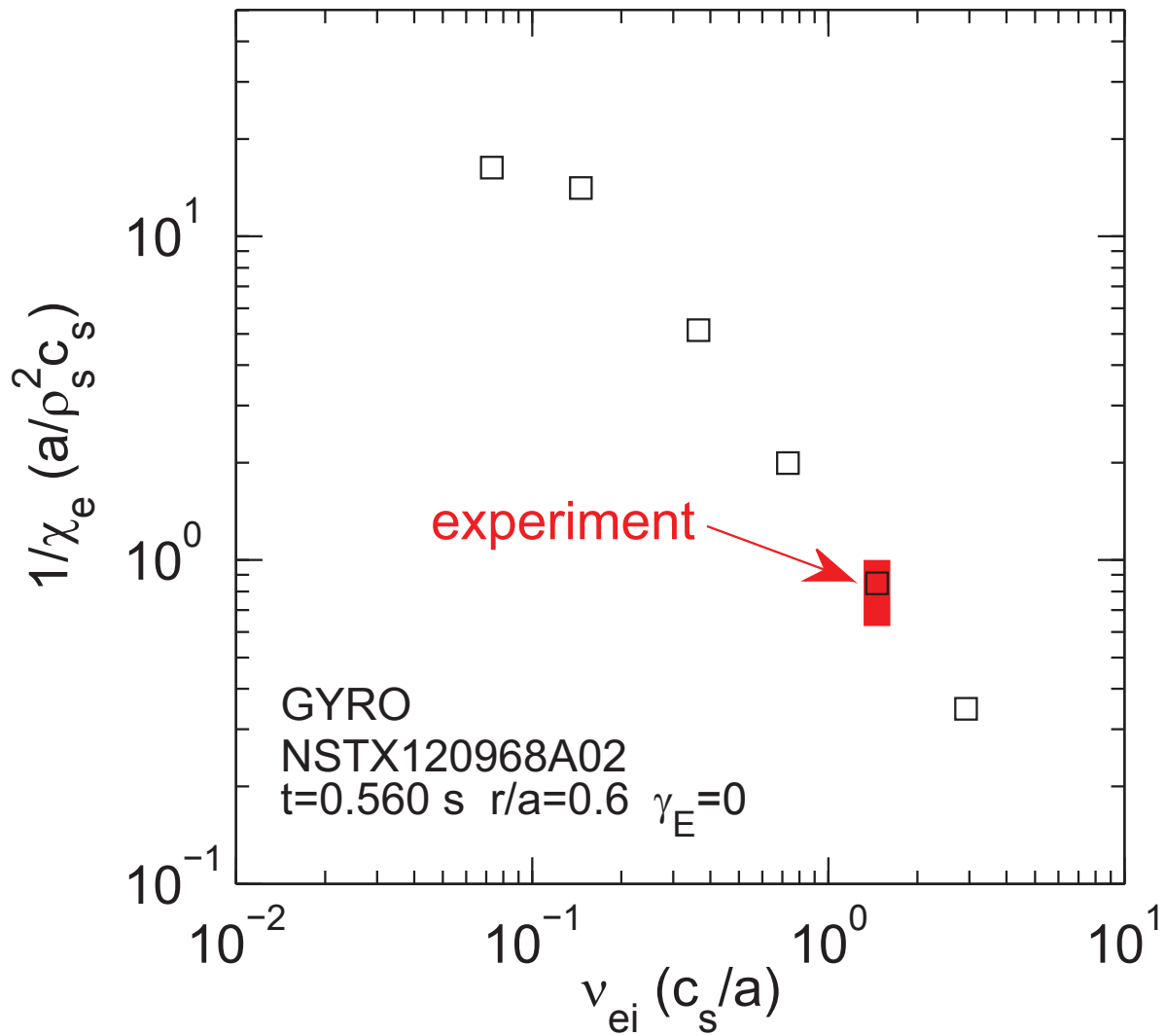


Figure 2. Nonlinear gyrokinetic simulations of the normalized inverse anomalous electron thermal diffusivity χ_e versus normalized collisionality for microtearing instabilities in NSTX.

NSTX Upgrade Scenarios														
Scenario	NSTX Reference		100% NICD		Long-pulse		Max I_p		Max I_p, P_{heat}		100% NICD		Max I_p	
			H98y2	H98y2	ST	ST	ST	ST						
Confinement scaling														
I_p [MA]	1.0	1.0	0.75	0.75	0.90	0.90	2.00	2.00	2.00	2.00	1.25	1.25	2.00	2.00
B_T [Tesla]	0.45	0.45	1.00	1.00	0.75	0.75	1.00	1.00	1.00	1.00	1.00	1.00	1.00	1.00
Aspect ratio	1.5	1.5	1.7	1.7	1.7	1.7	1.7	1.7	1.7	1.7	1.7	1.7	1.7	1.7
R_0 [m]	0.86	0.86	0.93	0.93	0.93	0.93	0.93	0.93	0.93	0.93	0.93	0.93	0.93	0.93
Elongation	2.8	2.8	2.80	2.80	2.80	2.80	2.80	2.80	2.80	2.80	2.80	2.80	2.80	2.80
Greenwald fraction	0.5	1.0	0.50	1.00	0.50	1.00	0.50	1.00	0.50	1.00	0.50	1.00	0.50	1.00
n_e -bar [10^{20}m^{-3}]	0.52	1.03	0.37	0.73	0.44	0.88	0.98	1.96	0.98	1.96	0.61	1.22	0.98	1.96
P_{NBI} [MW]	6.0	6.0	10.0	10.0	5.0	5.0	10.0	10.0	15.0	15.0	6.0	6.0	6.0	6.0
P_{RF} [MW]	0.0	0.0	0.0	0.0	0.0	0.0	0.0	0.0	6.0	6.0	0.0	0.0	0.0	0.0
P_{heat} [MW]	6.0	6.0	10.0	10.0	5.0	5.0	10.0	10.0	21.0	21.0	6.0	6.0	6.0	6.0
I_p flat-top time [s]	1.0	1.0	5.0	5.0	10.0	10.0	5.0	5.0	1.0	1.0	5.0	5.0	5.0	5.0
$\tau_{\text{current-redistribution}}$ [s]	0.25	0.19	0.44	0.34	0.33	0.25	0.69	0.53	0.96	0.74	1.31	0.82	1.14	0.71
# redistribution times	4.0	5.2	11.3	14.7	30.4	39.6	7.3	9.5	1.0	1.4	3.8	6.1	4.4	7.0
Stored energy [MJ]	0.29	0.29	0.51	0.39	0.30	0.29	0.84	0.97	1.14	1.25	0.88	0.84	1.09	1.15
β_N [%mT/MA]	5.4	5.5	5.9	4.5	3.8	3.8	3.7	4.2	5.0	5.4	6.1	5.8	4.7	5.0
β_T [%]	21.5	21.9	7.8	5.9	8.1	8.0	12.8	14.8	17.4	19.1	13.3	12.8	16.5	17.5
q^*	3.6	3.6	10.3	10.3	6.4	6.4	3.9	3.9	3.9	3.9	6.2	6.2	3.9	3.9
Fast-ion β fraction	0.33	0.14	0.62	0.35	0.37	0.15	0.19	0.07	0.25	0.10	0.25	0.10	0.12	0.04
v_e^* [$\times 10^2$] (for $q=2$)	5.8	16.3	2.38	6.75	4.23	12.0	3.52	10.0	2.26	6.40	0.93	3.48	1.80	6.73
Bootstrap fraction	0.36	0.47	0.66	0.87	0.45	0.59	0.33	0.44	0.41	0.55	0.81	0.93	0.46	0.53
NBI CD fraction	0.06	0.02	0.34	0.14	0.10	0.04	0.07	0.03	0.12	0.05	0.20	0.07	0.07	0.03
Non-inductive fraction	0.41	0.49	1.00	1.01	0.55	0.64	0.40	0.46	0.54	0.60	1.01	1.01	0.53	0.56
I_p ramp-up time [s]	0.2	0.2	0.38	0.38	0.45	0.45	1.00	1.00	1.00	1.00	0.63	0.63	1.00	1.00
I_p ramp-down time [s]	0.1	0.1	0.19	0.19	0.23	0.23	0.50	0.50	0.50	0.50	0.31	0.31	0.50	0.50
Total I_p duration [s]	1.3	1.3	5.6	5.6	10.7	10.7	6.5	6.5	2.5	2.5	5.9	5.9	6.5	6.5
TF flat-top time [s]	1.3	1.3	6.6	6.6	11.7	11.7	6.6	6.6	6.6	6.6	6.6	6.6	6.6	6.6
Fraction TF flat-top used	0.97	0.97	0.84	0.84	0.91	0.91	0.98	0.98	0.38	0.38	0.90	0.90	0.98	0.98
Total OH flux [Wb]	0.75	0.75	2.10	2.10	2.10	2.10	2.10	2.10	2.10	2.10	2.10	2.10	2.10	2.10
I_p ramp-up flux [Wb]	0.37	0.37	0.30	0.30	0.36	0.36	0.80	0.80	0.80	0.80	0.50	0.50	0.80	0.80
Surface voltage [V]	0.24	0.26	0.00	0.00	0.13	0.14	0.19	0.22	0.10	0.12	0.00	0.00	0.09	0.13
Total flat-top flux [Wb]	0.38	0.38	1.80	1.80	1.74	1.74	1.30	1.30	1.30	1.30	1.60	1.60	1.30	1.30
Flat-top flux used [Wb]	0.24	0.26	0.00	0.0	1.33	1.40	0.95	1.09	0.10	0.12	0.0	0.0	0.44	0.67
Fraction OH flux used	0.81	0.84	0.14	0.14	0.81	0.84	0.83	0.90	0.43	0.44	0.24	0.24	0.59	0.70
Power fraction to divertor	0.5	0.5	0.50	0.50	0.50	0.50	0.50	0.50	0.50	0.50	0.50	0.50	0.50	0.50
$R_{\text{strike-point}}$ [m]	0.40	0.40	0.50	0.50	0.50	0.50	0.50	0.50	0.50	0.50	0.50	0.50	0.50	0.50
SOL heat-flux width [cm]	0.90	0.90	1.43	1.43	1.07	1.07	0.30	0.30	0.30	0.30	0.63	0.63	0.30	0.30
Poloidal flux expansion	22.0	22.0	20.0	20.0	20.0	20.0	62.0	62.0	58.0	58.0	20.0	20.0	37.0	37.0
Peak heat flux [MW/m^2]	6.0	6.0	5.6	5.6	3.7	3.7	8.6	8.6	13.9	13.9	7.6	7.6	8.7	8.7
Time to $T_{\text{PFC}} = 1200^\circ\text{C}$ [s]	13.8	13.8	16.1	16.1	35.8	35.8	6.7	6.7	2.6	2.6	8.7	8.7	6.6	6.6
Fraction of T_{PFC} limit	0.09	0.09	0.35	0.35	0.30	0.30	0.97	0.97	0.96	0.96	0.68	0.68	0.98	0.98

Table 1. Parameters of representative NSTX-U scenarios.

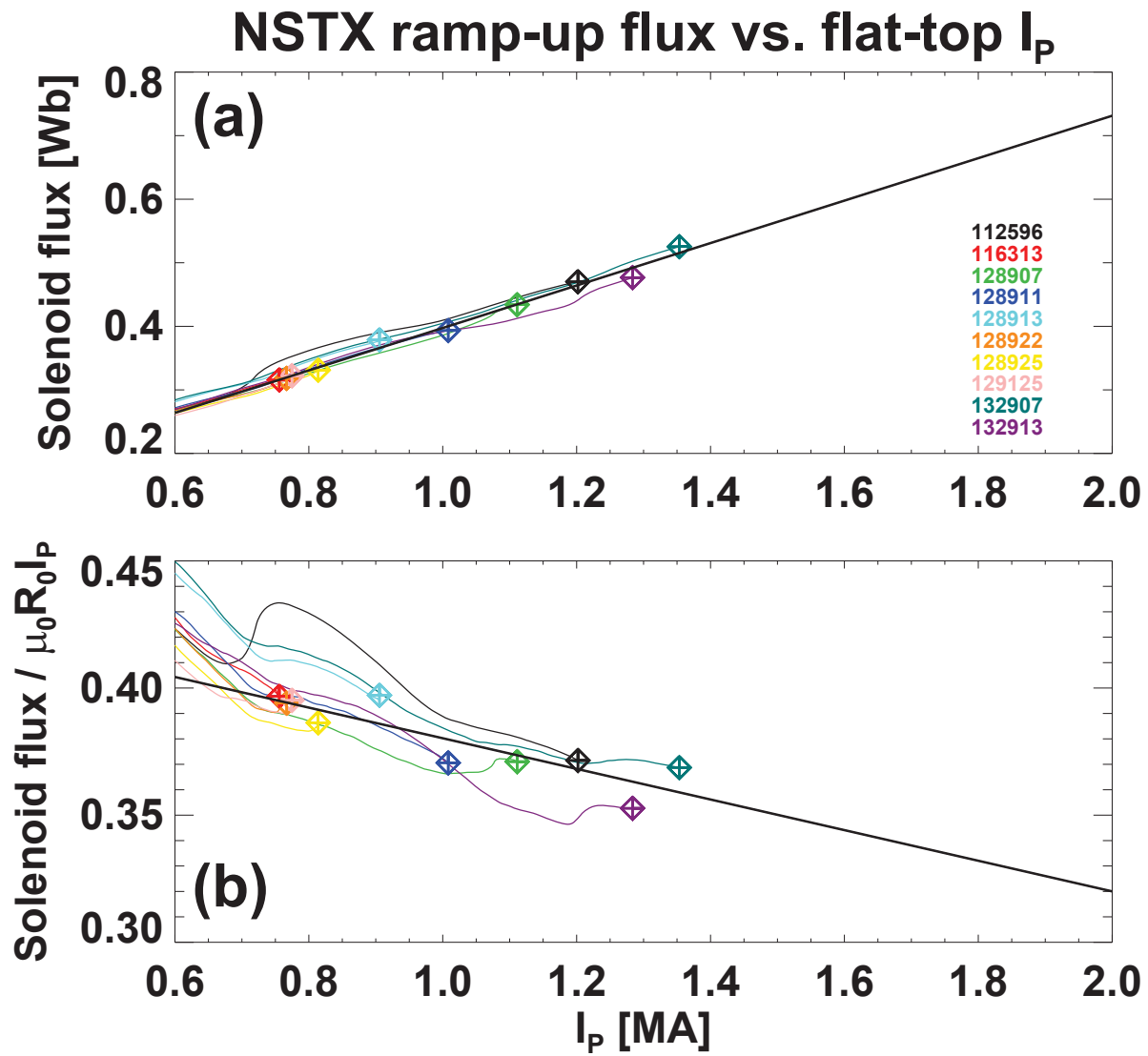


Figure 3. (a) Solenoid flux consumed for break-down and ramp-up vs. plasma current flat-top value, and (b) normalized flux consumed (Ejima-Wesley coefficient) vs. current flat-top value.

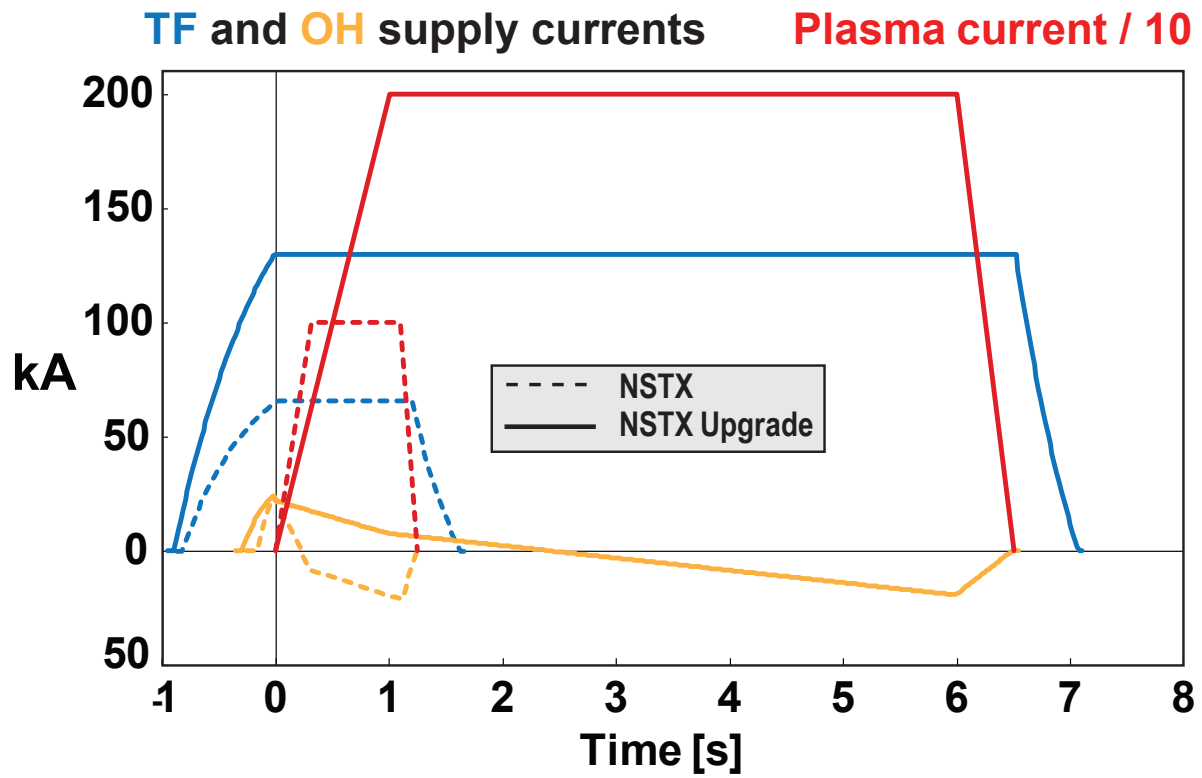
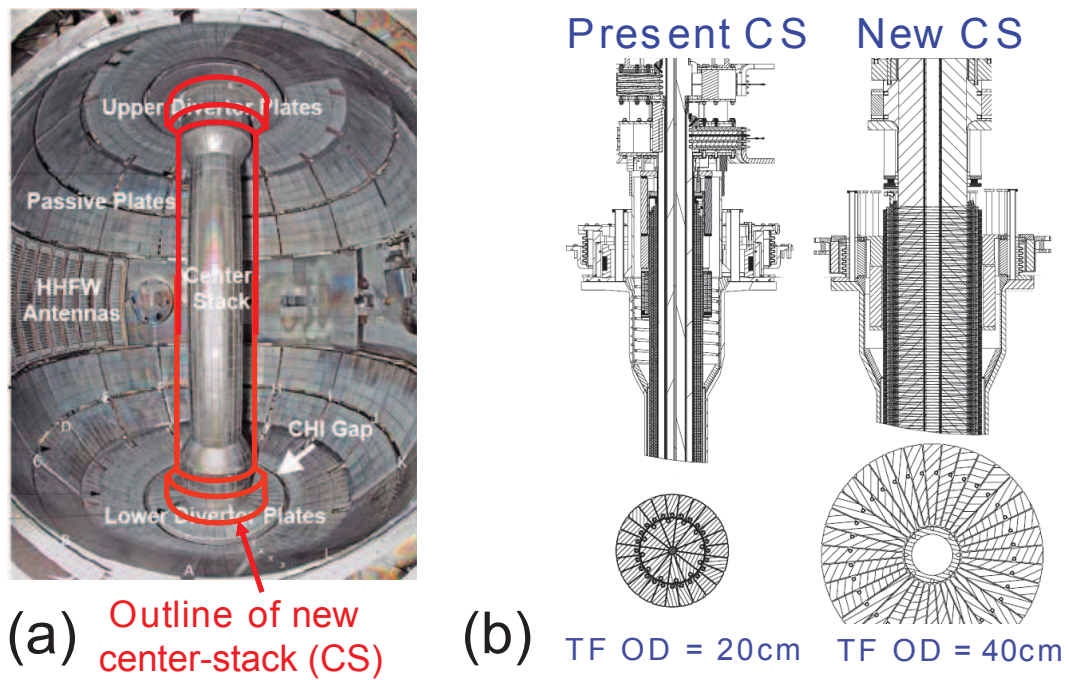
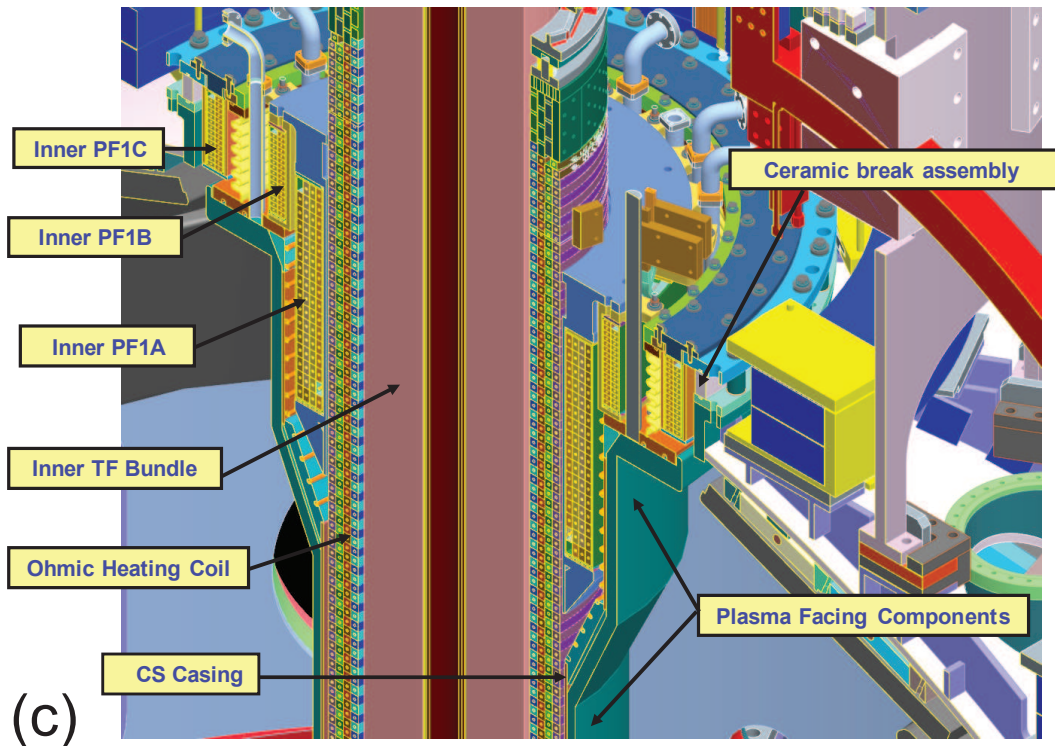


Figure 4. Comparison of toroidal field (TF), ohmic heating (OH), and plasma current waveforms for plasmas operated at the maximum toroidal field capabilities of NSTX (0.55T) and NSTX Upgrade (1T).



(a) Outline of new center-stack (CS)

(b) TF OD = 20cm TF OD = 40cm



(c)

Figure 5. (a) Outlines and (b) cross-sections of the present and new center-stack for comparing the TF conductor diameters, and (c) detailed cross-section of the Upgrade center-stack showing the TF, OH, and divertor PF coils, and the CHI insulator and PFC boundaries.

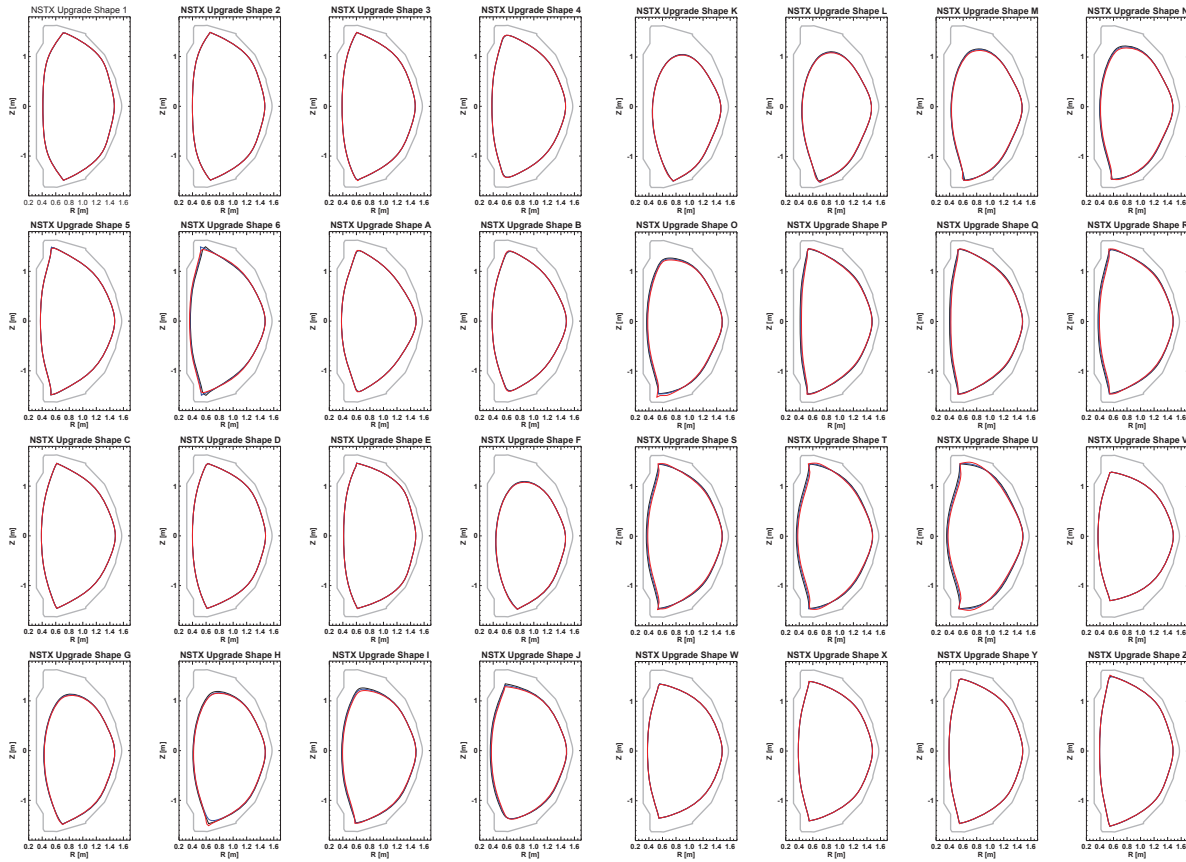


Figure 6. Plasma boundaries of free-boundary equilibria used for assessing PF coil current requirements in NSTX Upgrade. Each plot is a superposition of three boundary plots, i.e. one for each OH power supply current state assessed: 0kA and ± 24 kA.

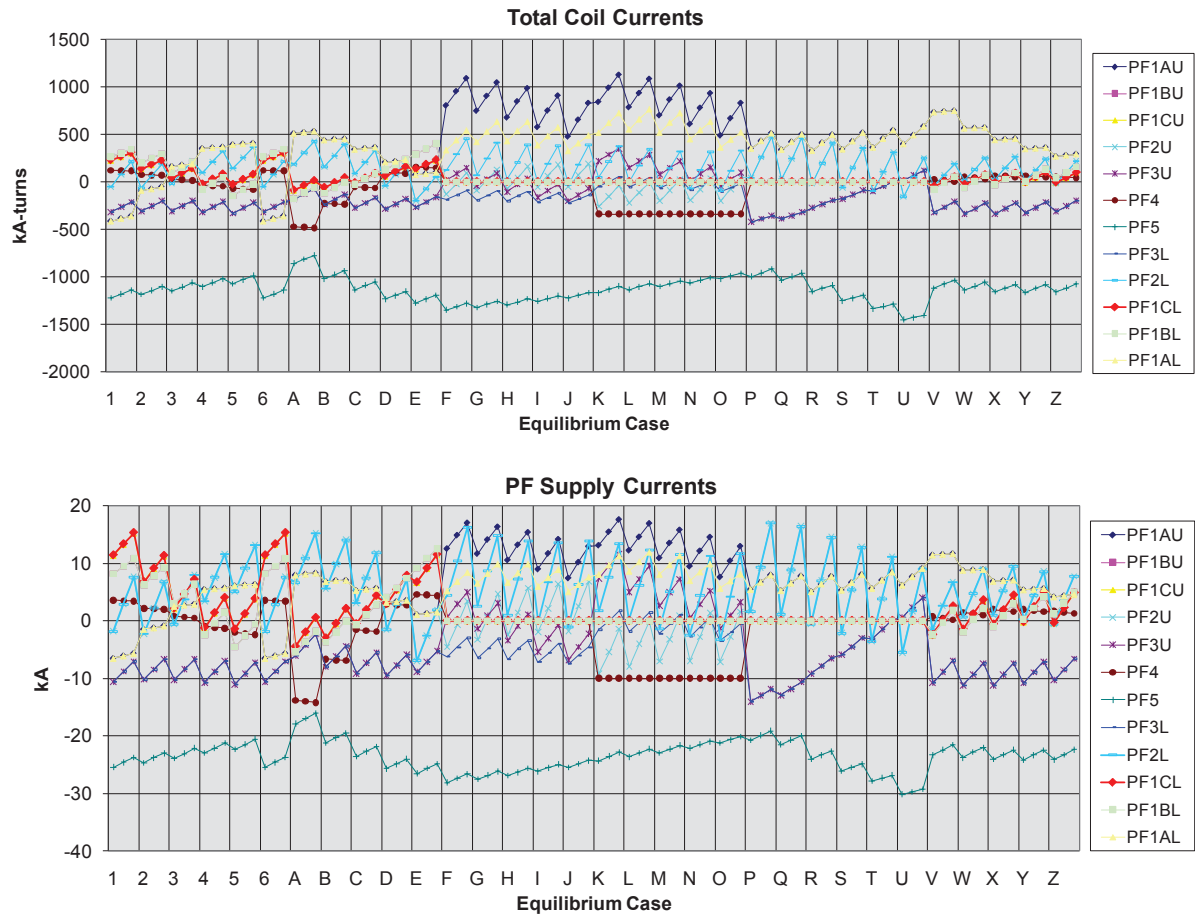


Figure 7. Total coil current (top) and power supply current (bottom) required for each of the 96 reference 2MA Upgrade equilibria.

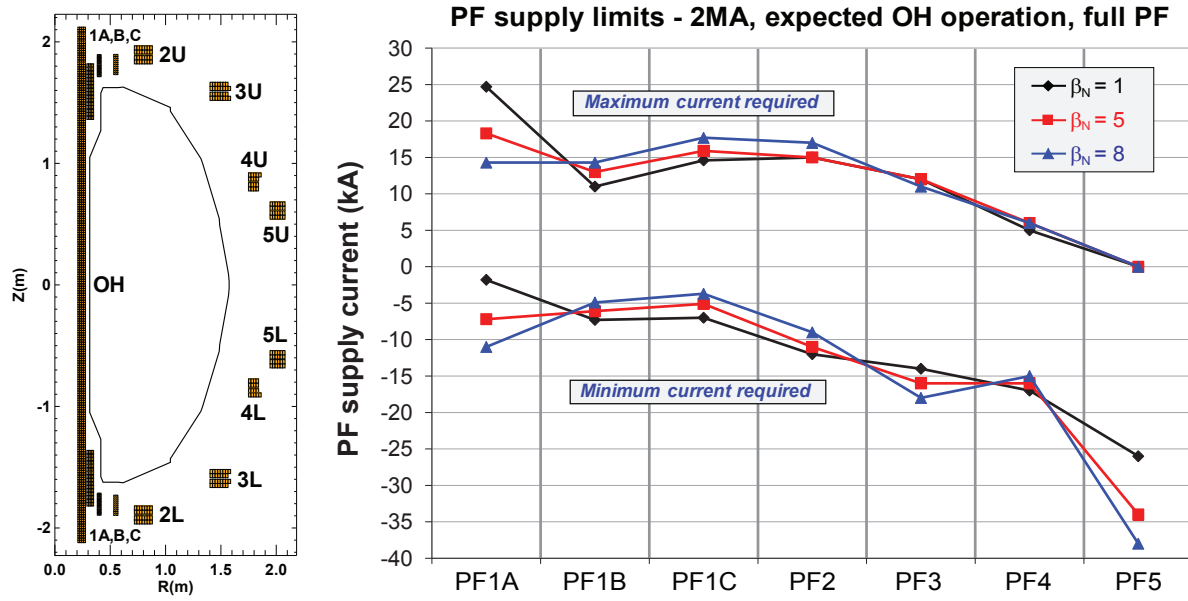


Figure 8. (Left) PF and OH coil current locations, sizes, and limiter boundary and (right) minimum and maximum PF coil current vs β_N .

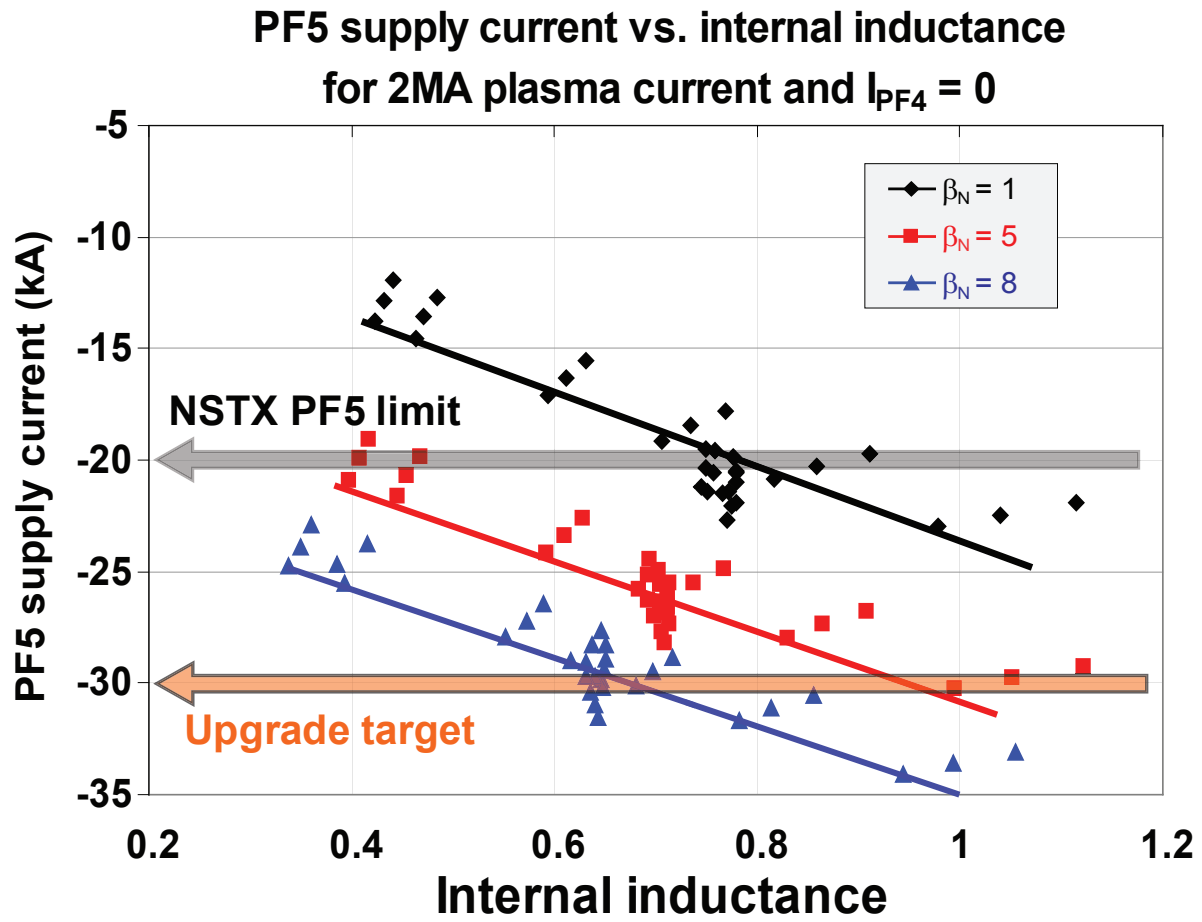


Figure 9. PF5 vertical field coil current required to support 2MA plasmas as a function of internal inductance and normalized beta.

Coil	NR	NZ	Turns	Equilibrium multiplier	Min power supply kA	Max power supply kA	Min coil MA turns	Max coil MA turns
OH	4.0	221	884	1.0	-24.0	24.0	-21.2	21.2
PF1AU,L	4.0	16	64	1.1	-7.2	18.3	-0.46	1.17
PF1BU,L	2.0	16	32	1.1	-6.0	13.0	-0.19	0.42
PF1CU,L	2.0	10	20	1.1	-5.0	15.9	-0.10	0.32
PF2U,L	7.0	4	28	1.1	-11.0	15.0	-0.31	0.42
PF3U,L	7.5	4	30	1.1	-16.0	12.0	-0.48	0.36
PF4	8.5	4	34	1.1	-16.0	6.0	-0.54	0.20
PF5	6.0	8	48	1.1	-34.0	0.0	-1.63	0.00

Table 2. NSTX Upgrade OH and PF coil number of radial layers (NR), vertical layers (NZ), total turns-count, power supply current multiplier with respect to the required equilibrium current, and minimum and maximum power supply and total coil currents.

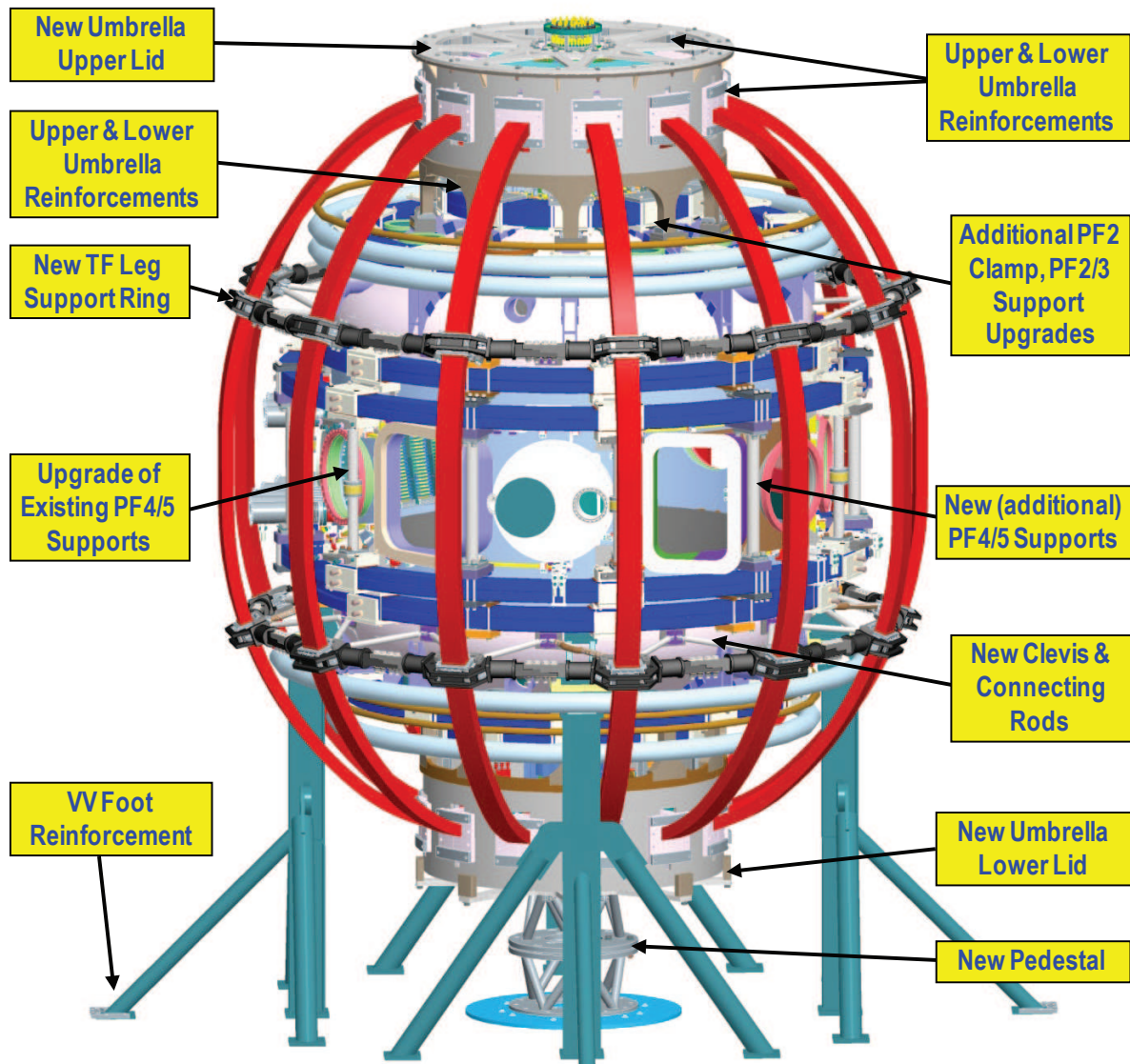


Figure 10. Vessel reinforcements and other modifications required for handling the increased forces associated with higher field and current of NSTX Upgrade.

Lower OH coil winding

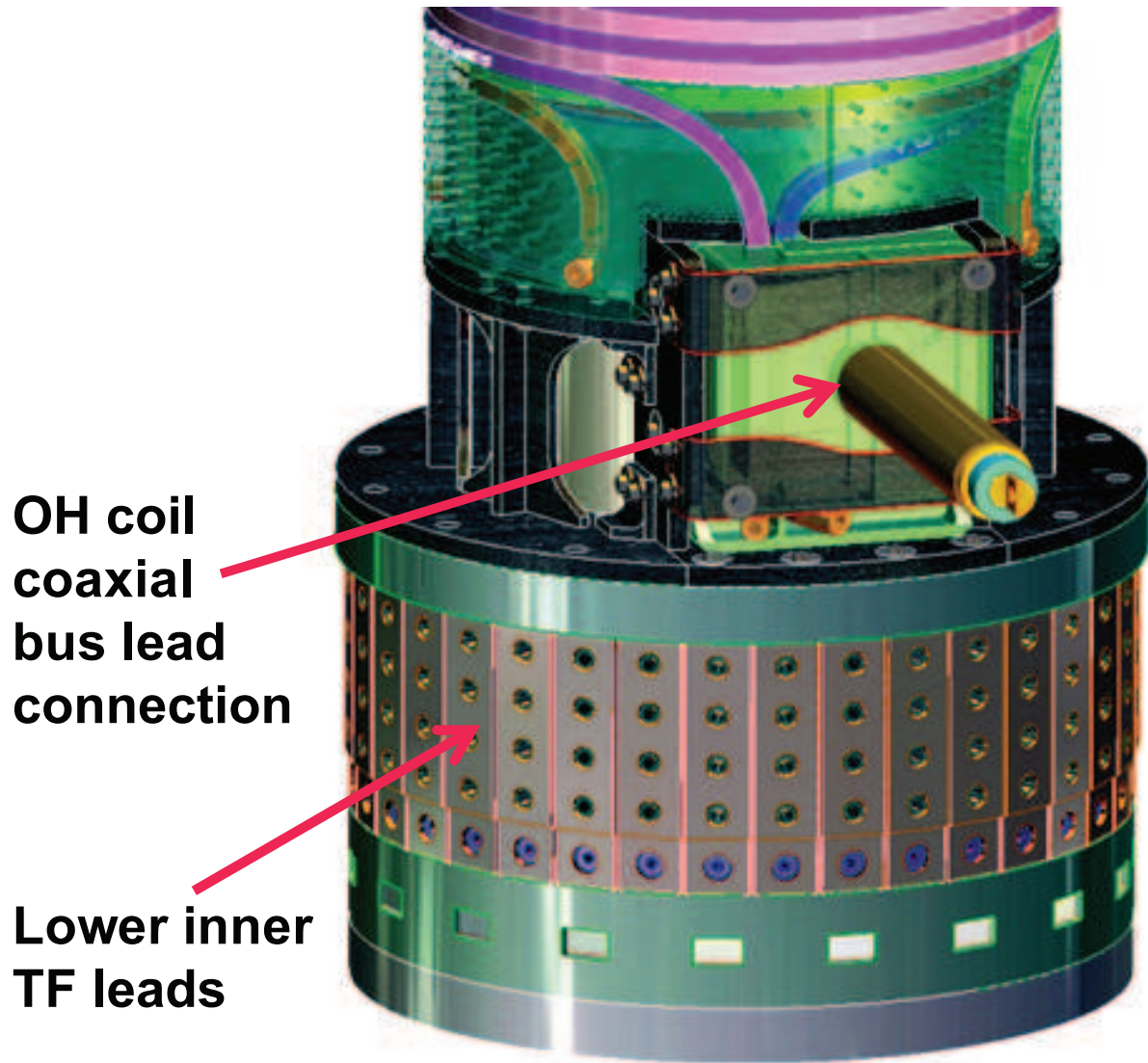


Figure 11. Design drawing of the lower OH coil winding area including the coaxial bus lead connection and lower inner TF leads.

Acceleration Voltage [kV]	MW per Source	MW per Beamline	Pulse Length [s]
65	1.1	3.2	8
70	1.3	3.8	7
75	1.5	4.5	6
80	1.7	5.1	5
85	1.9	5.8	4
90	2.1	6.4	3
95	2.4	7.1	2
100	2.6	7.7	1.5
105	2.8	8.4	1.25
110	3.0	9.0	1

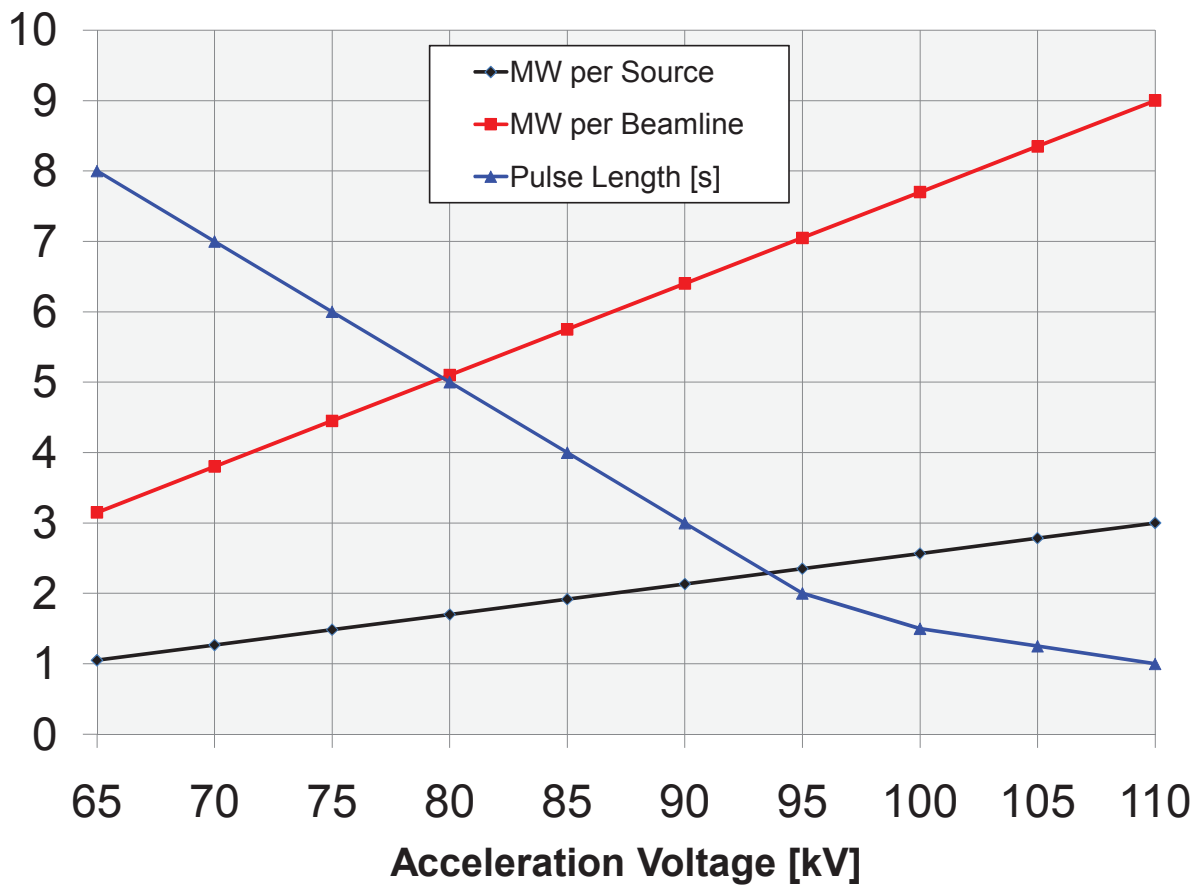
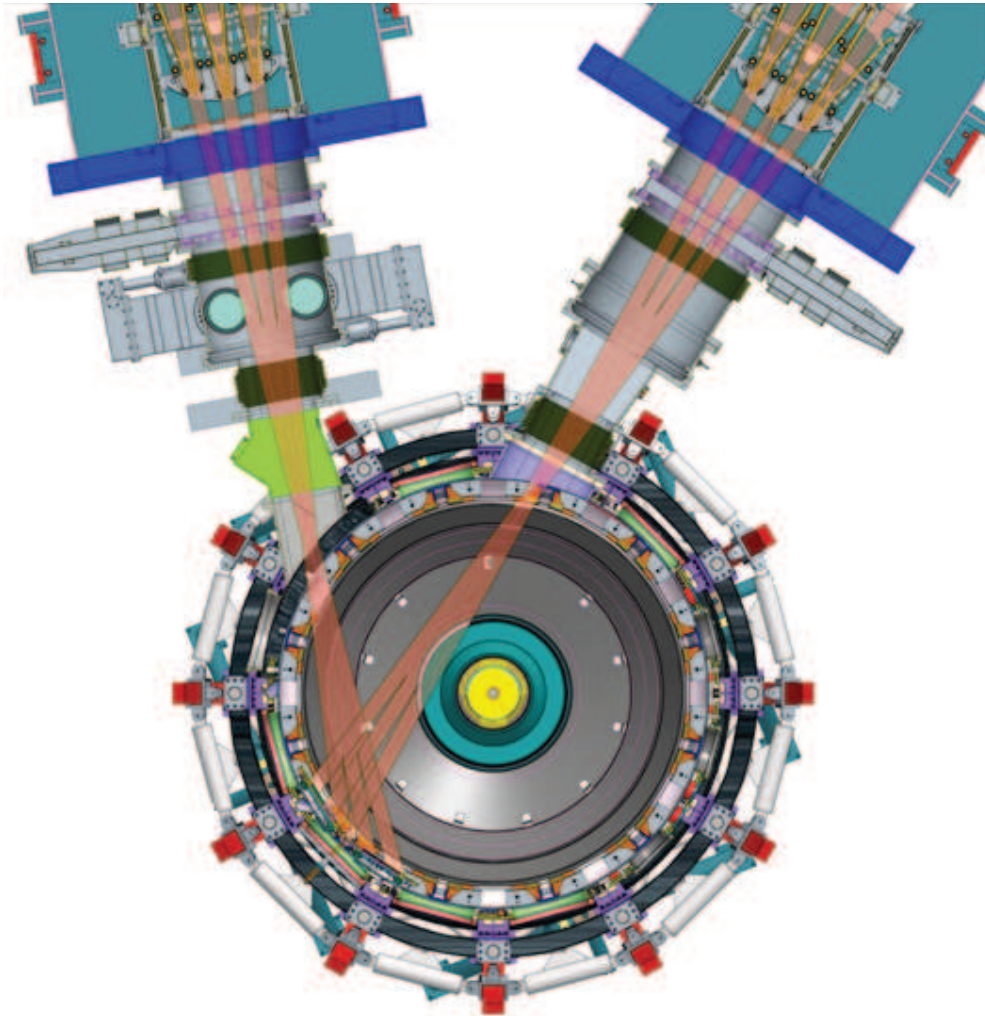


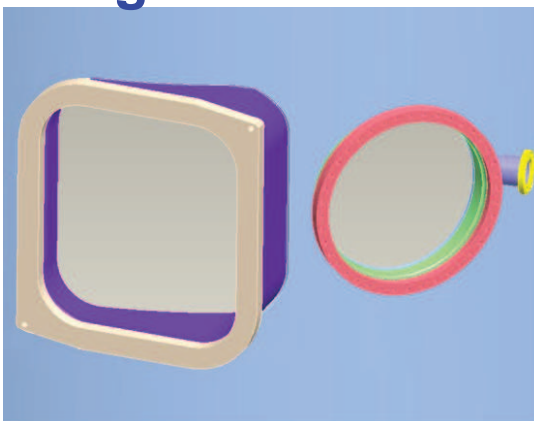
Figure 12. NSTX NBI power per source, power per beamline, and nominal maximum pulse-length versus NBI acceleration voltage.

(a) **New 2nd NBI** ($R_{\text{TAN}}=110, 120, 130\text{cm}$) **Present NBI** ($R_{\text{TAN}} = 50, 60, 70\text{cm}$)



(b)

Original NBI Port



New NBI Port

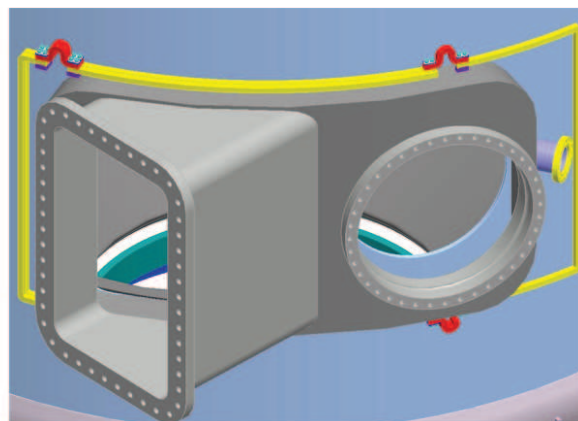


Figure 13. (a) Injection geometry of present and new 2nd NBI, and (b) modification of the present NBI port to a new NBI port cap to enable the more tangential injection.

NSTX

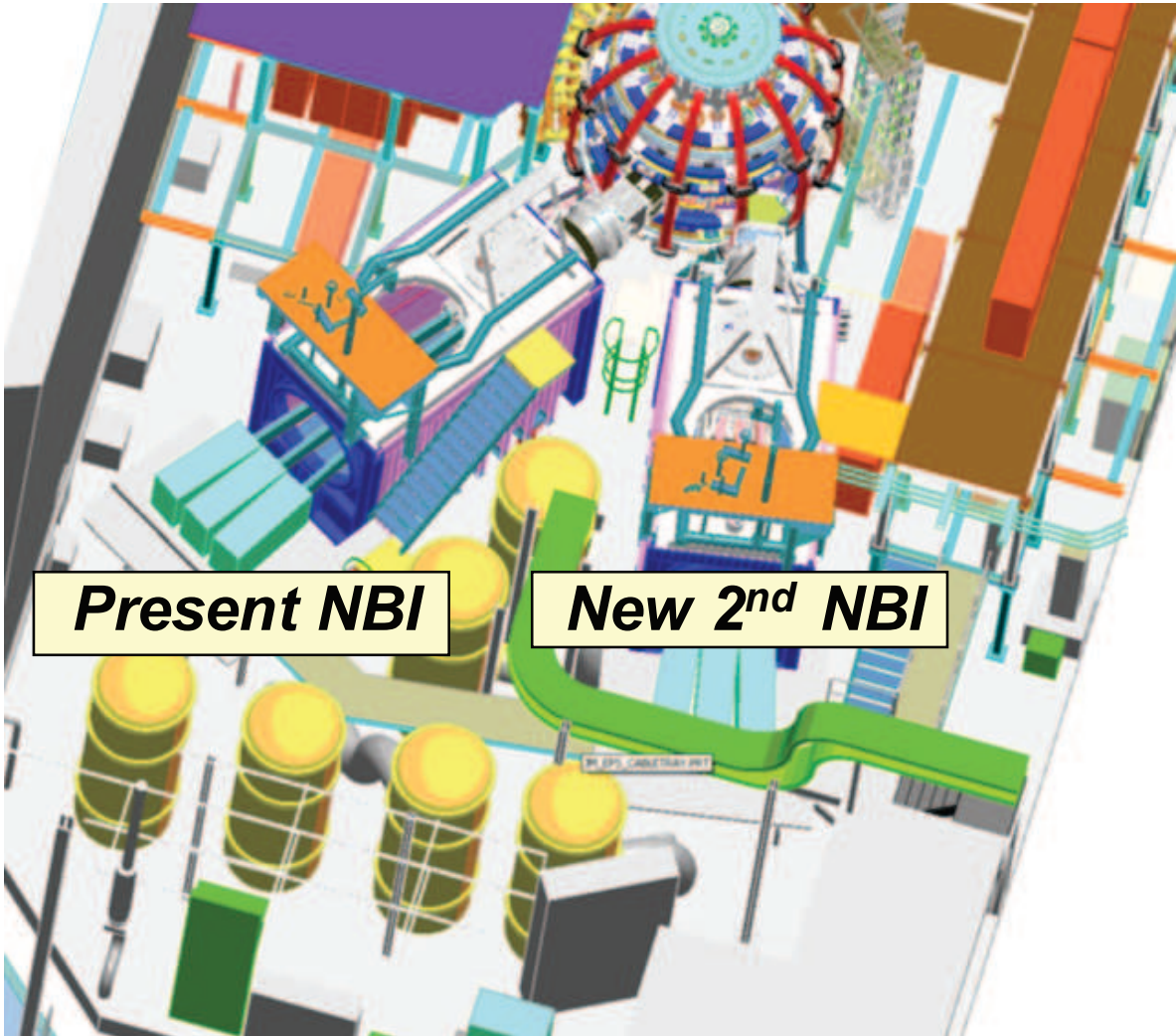


Figure 14. Drawing of top-down view of layout of NSTX test cell after installation of new 2nd NBI.

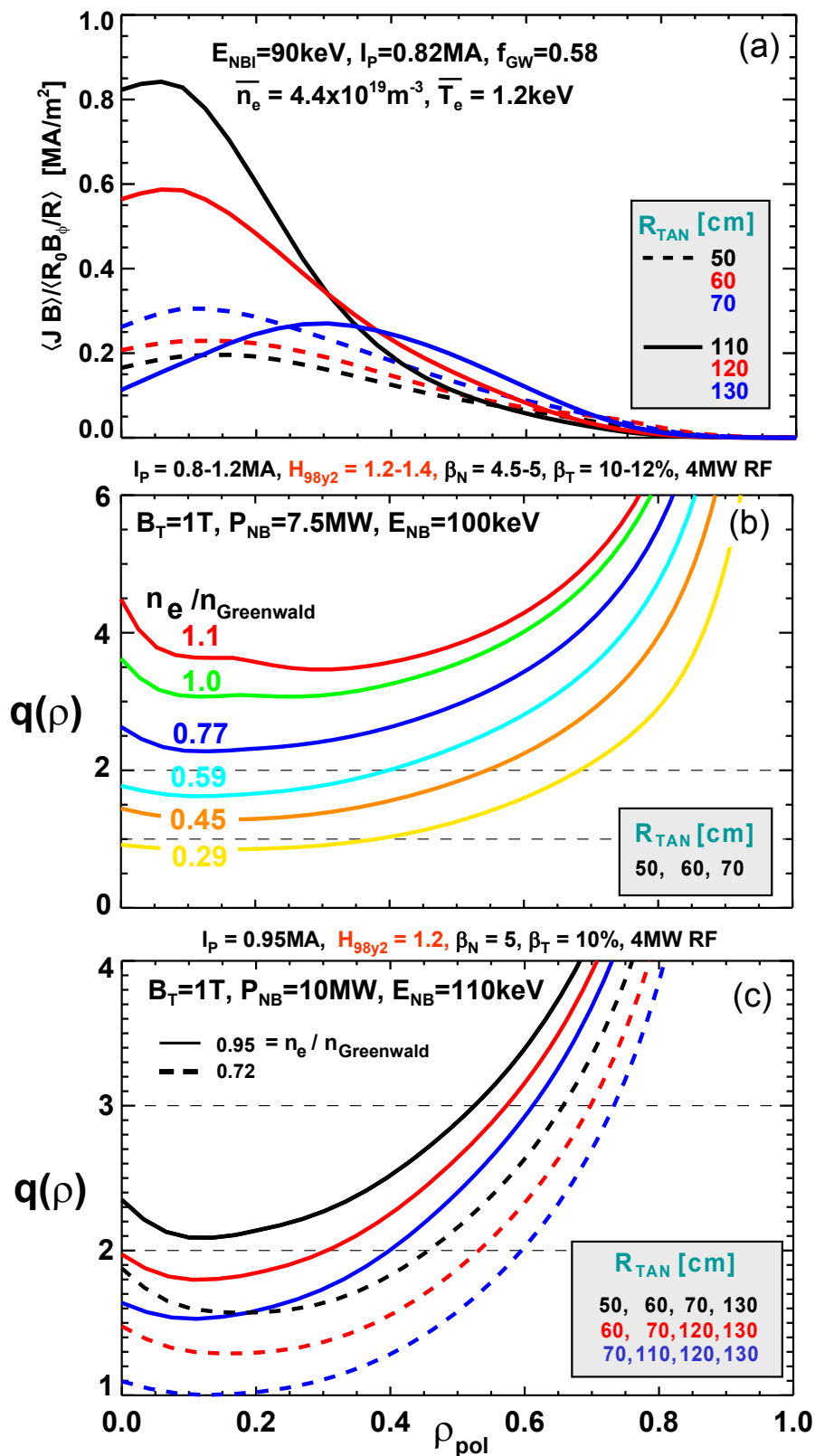
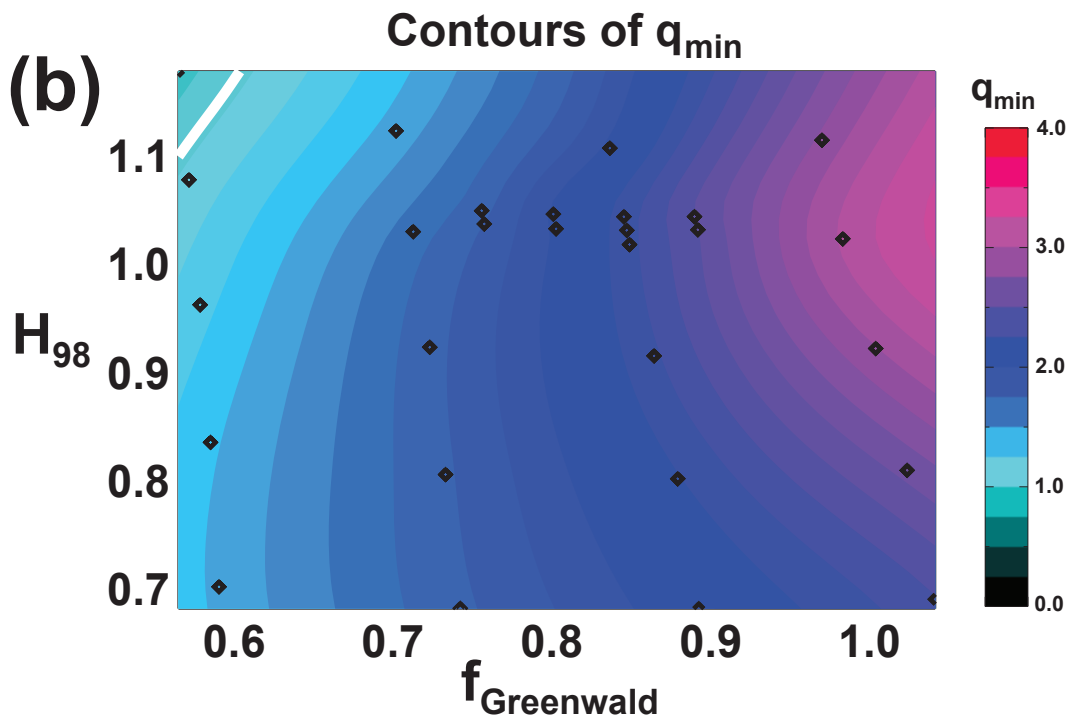
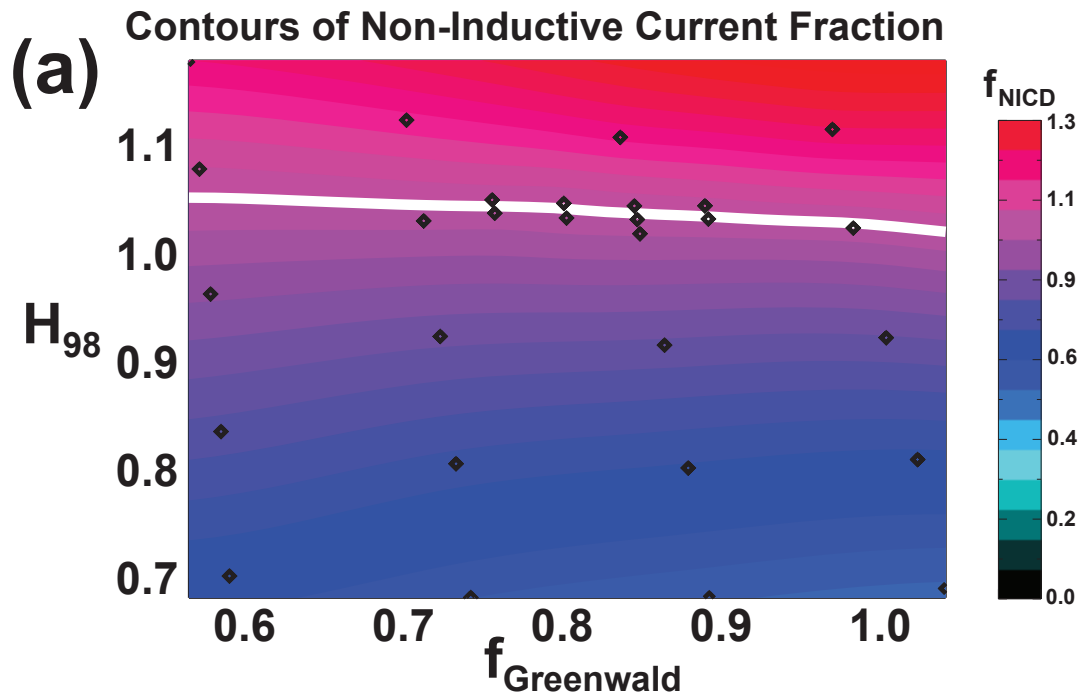


Figure 15. (a) Comparison of parallel current density profiles for existing (dashed) and 2nd (solid) NBI sources, and q profile controllability vs. density for (b) existing and (c) additional NBI sources.



$A=1.75, \kappa=2.8, B_T=1.0T, I_p=1.0MA$

90 kV Beams $R_{tan} = [50, 60, 70, 110, 120, 130]$ cm

Figure 16. Contours of (a) non-inductive current fraction and (b) minimum safety factor q_{min} versus $f_{Greenwald}$ and ITER H-mode confinement multiplier H_{98} for 1MA plasmas with 12MW of NBI heating.

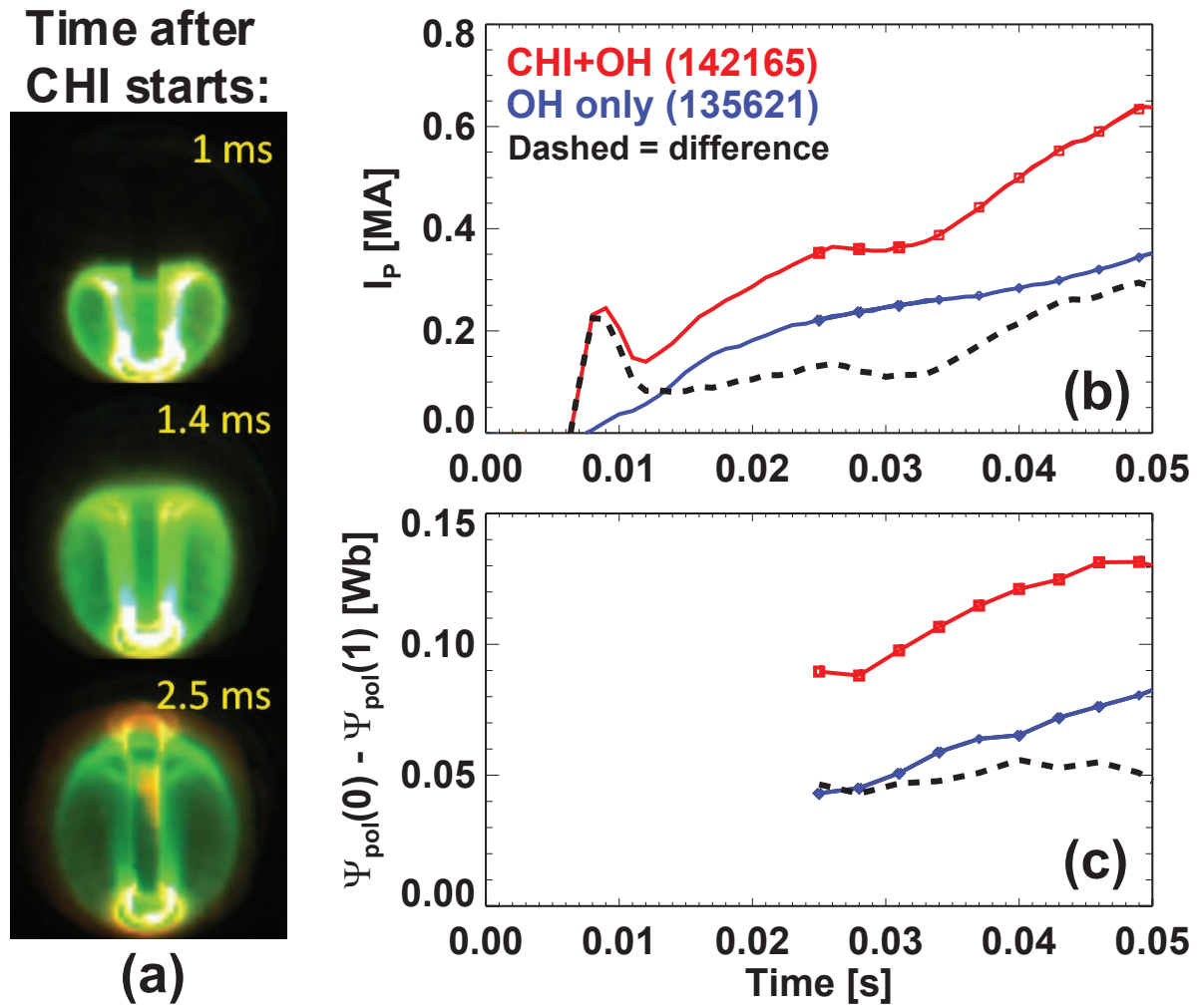


Figure 17. (a) Evolution of CHI plasma boundary light shortly after plasma formation, (b) plasma current savings and (c) poloidal flux savings from CHI coupled to induction in NSTX start-up plasmas.

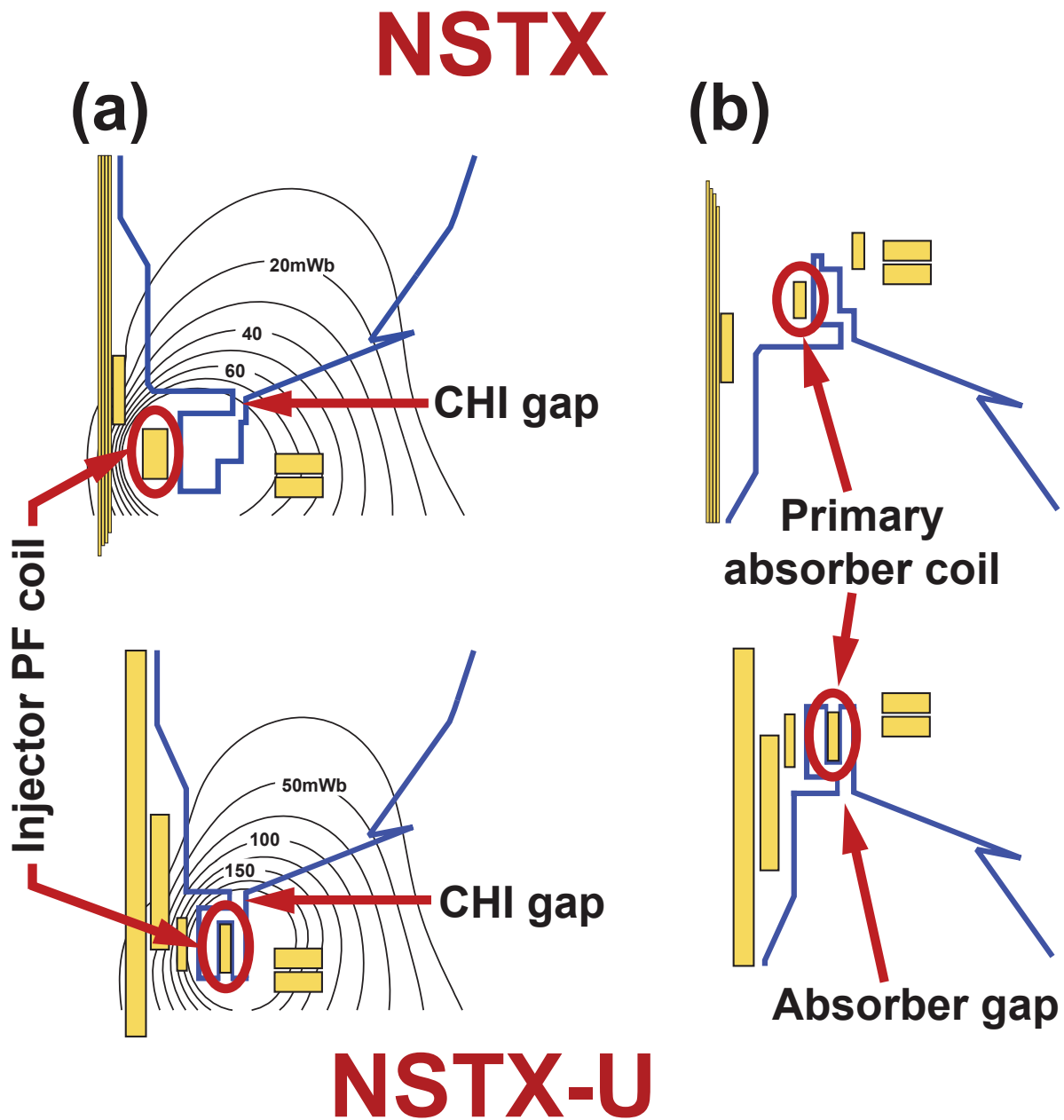


Figure 18. (a) Poloidal flux contours in the injector region of NSTX (top) and NSTX-U (bottom), and (b) field-nulling and divertor coils in the absorber region for CHI experiments.

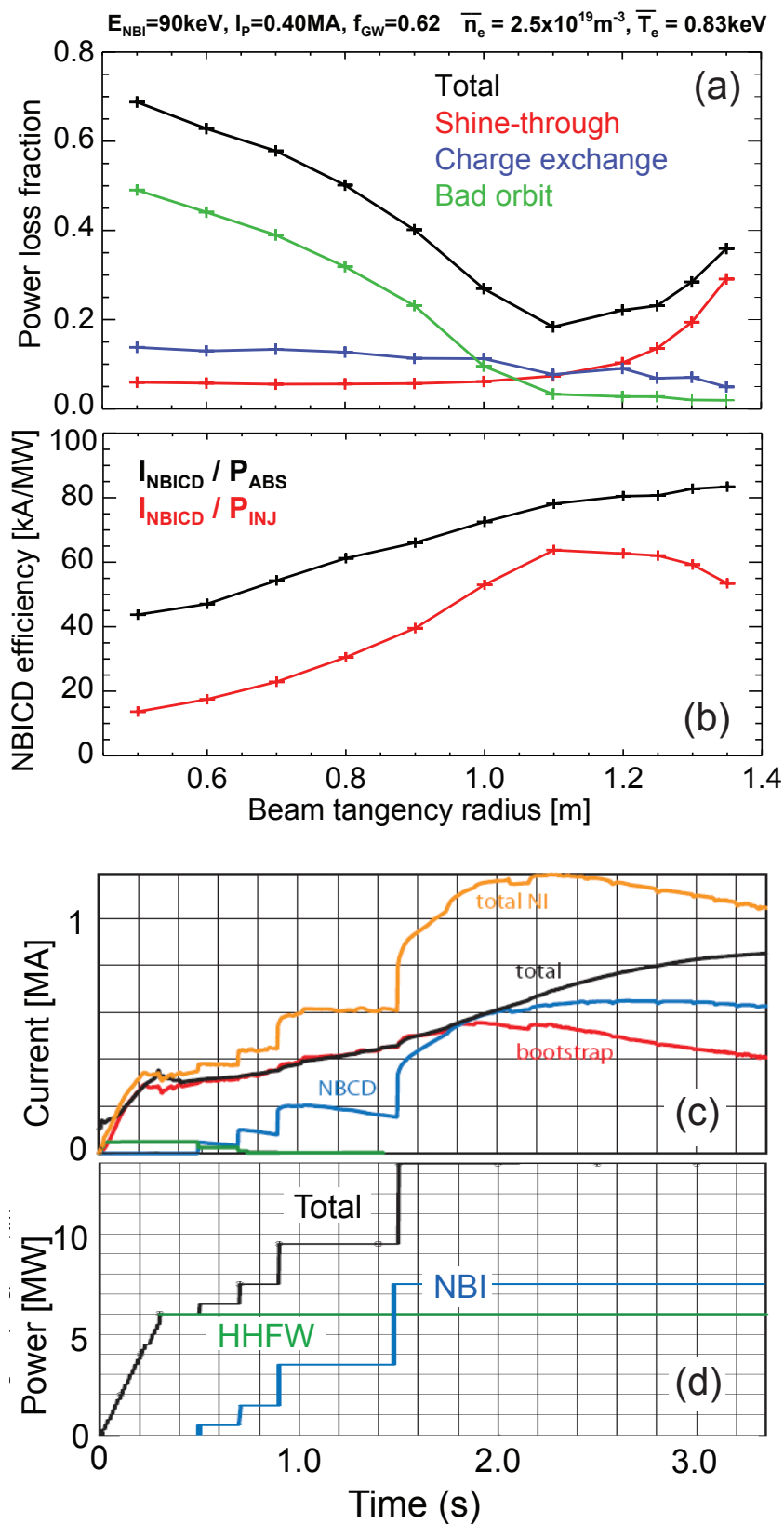


Figure 19. Predicted (TRANSP) (a) power loss fraction and (b) current drive efficiency vs. tangency radius, and simulated (TSC) (c) non-inductive currents and (d) heating power for non-inductive ramp-up.

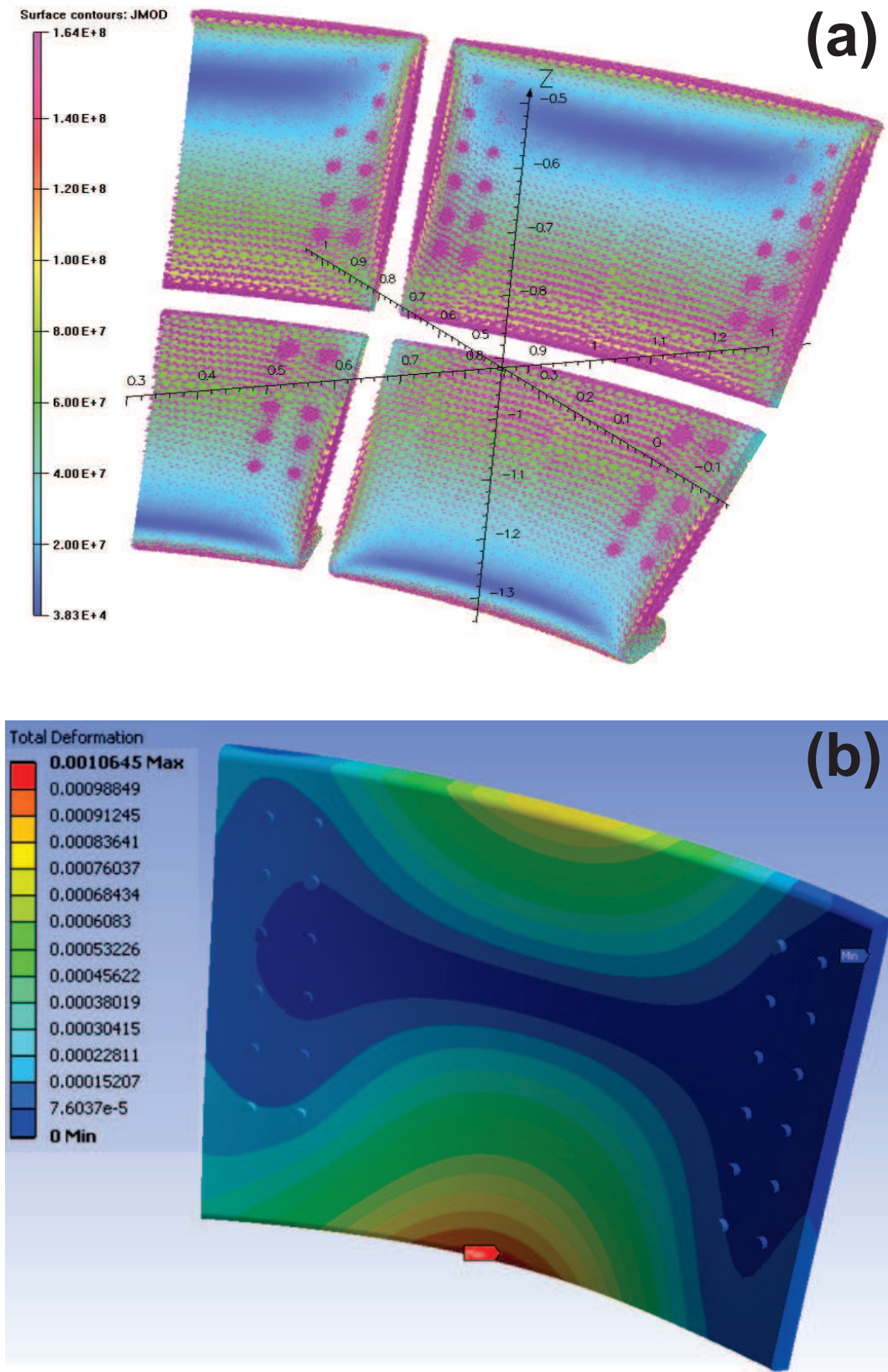


Figure 20. (a) Passive plate current density [A/m²] and (b) primary passive plate deflection [m] during a simulated downward VDE.

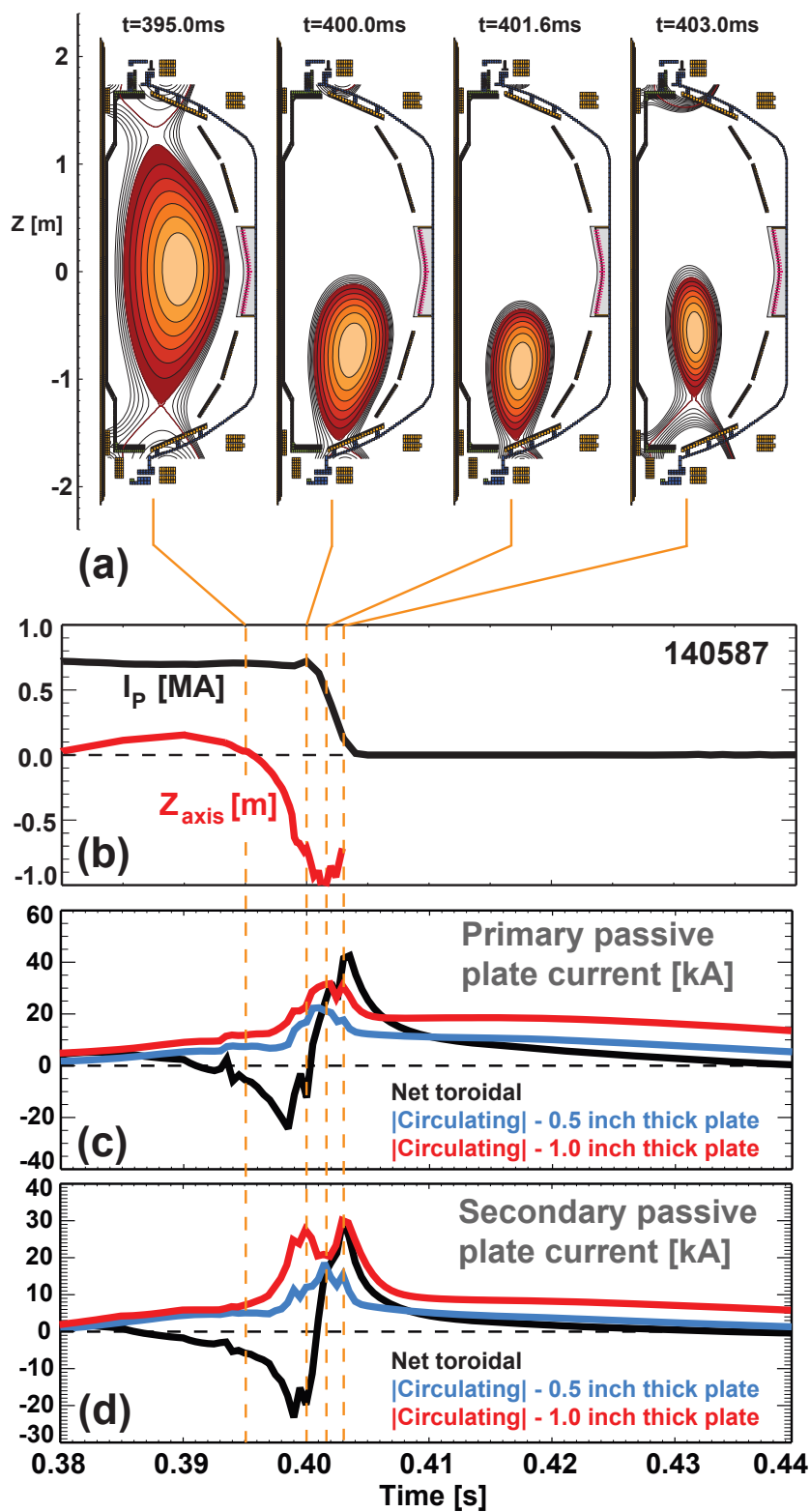


Figure 21. (a) Plasma position and shape evolution, (b) plasma current and magnetic axis position, (c) primary passive plate currents and (d) secondary passive plate currents during a vertical displacement event (VDE) and current quench in NSTX.

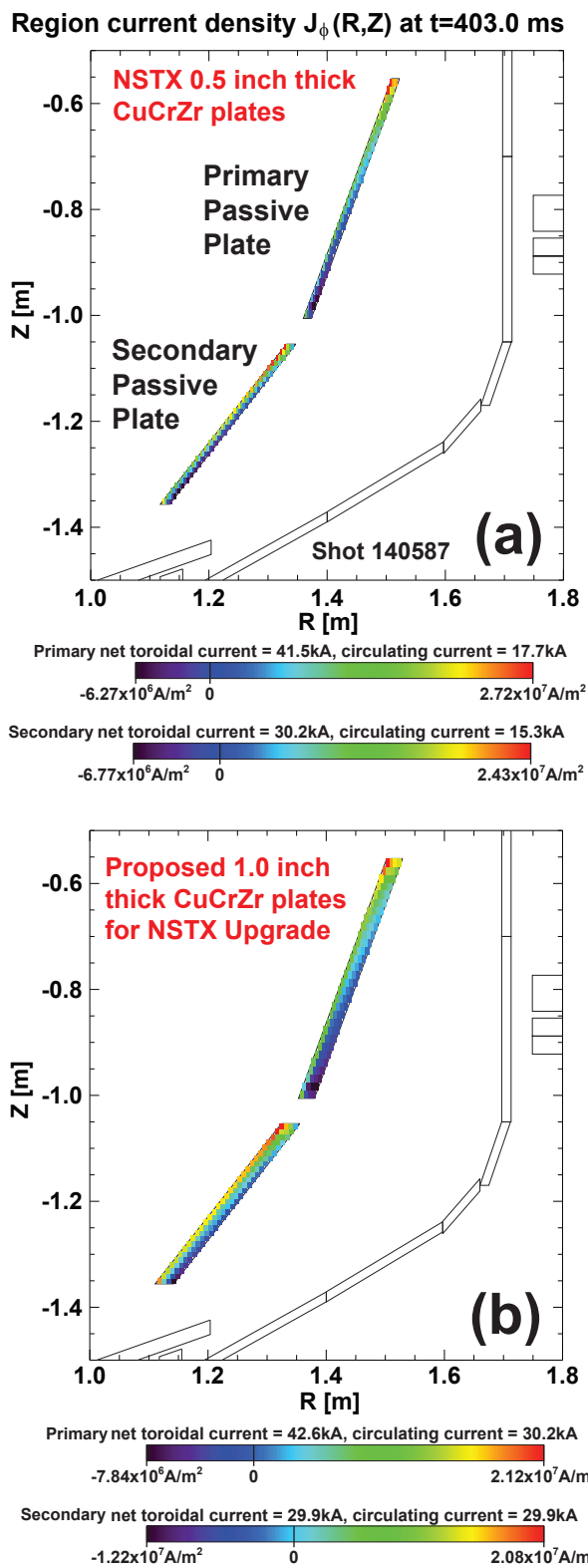


Figure 22. Toroidal current density in the primary and secondary passive plates at the time of peak net toroidal current and near the time of peak circulating current for (a) the present NSTX passive plates and (b) thicker passive plates being assessed for NSTX Upgrade for the shot shown in Figure 21.

VALEN model of NSTX Upgrade
(a) passive conducting structure

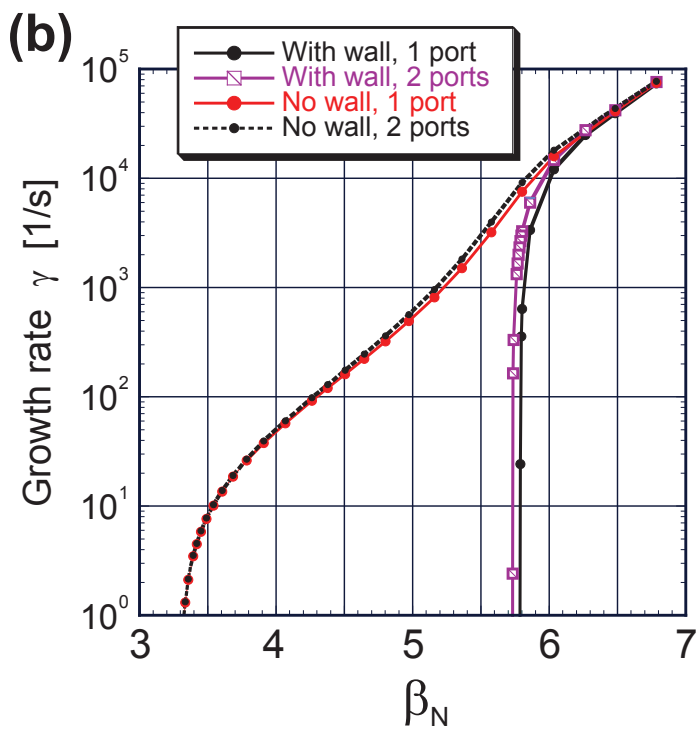
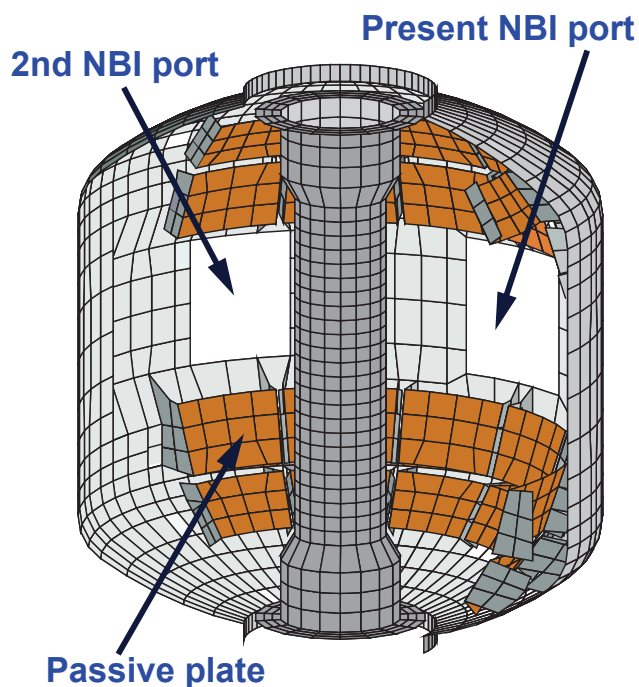


Figure 23. (a) VALEN model of the NSTX Upgrade passive conducting structure including the vessel cut-outs for the present and 2nd NBI ports and (b) predicted $n=1$ RWM growth rate vs. β_N for one and two vessel penetrations for NBI ports.

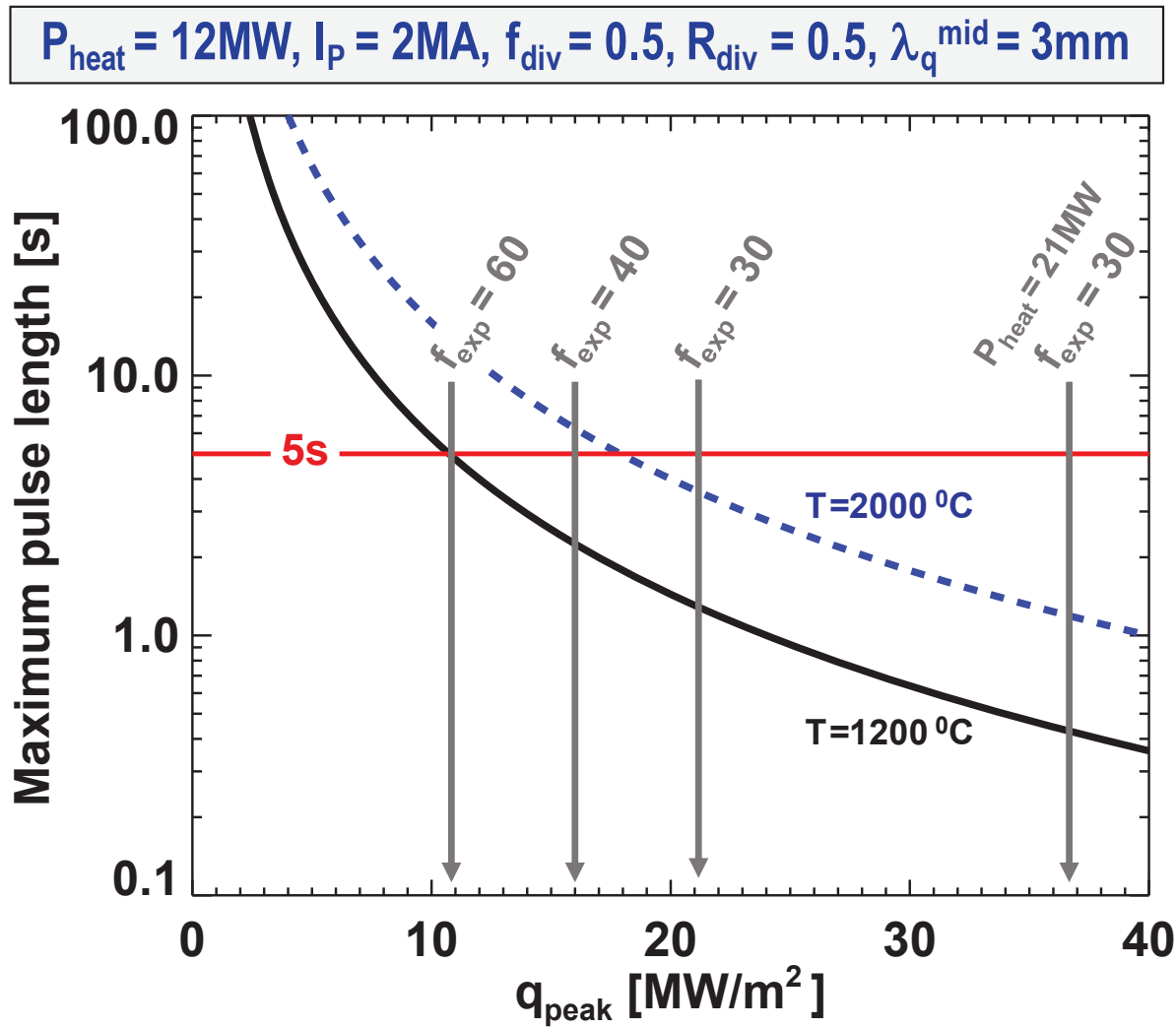


Figure 24. Projected NSTX Upgrade pulse-length limits versus peak divertor heat flux for two divertor carbon PFC temperature values.

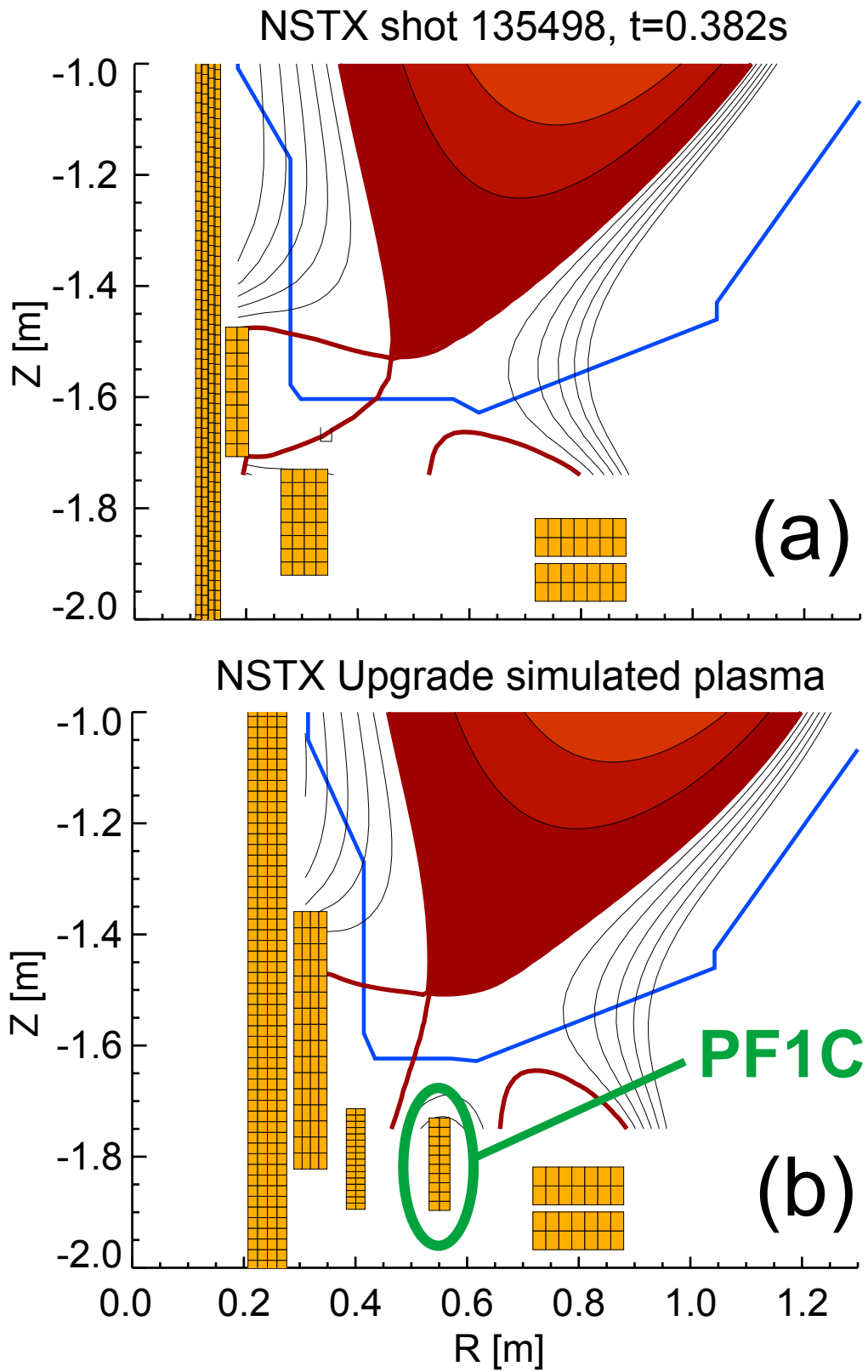


Figure 25. (a) Snowflake divertor in NSTX and (b) NSTX Upgrade.

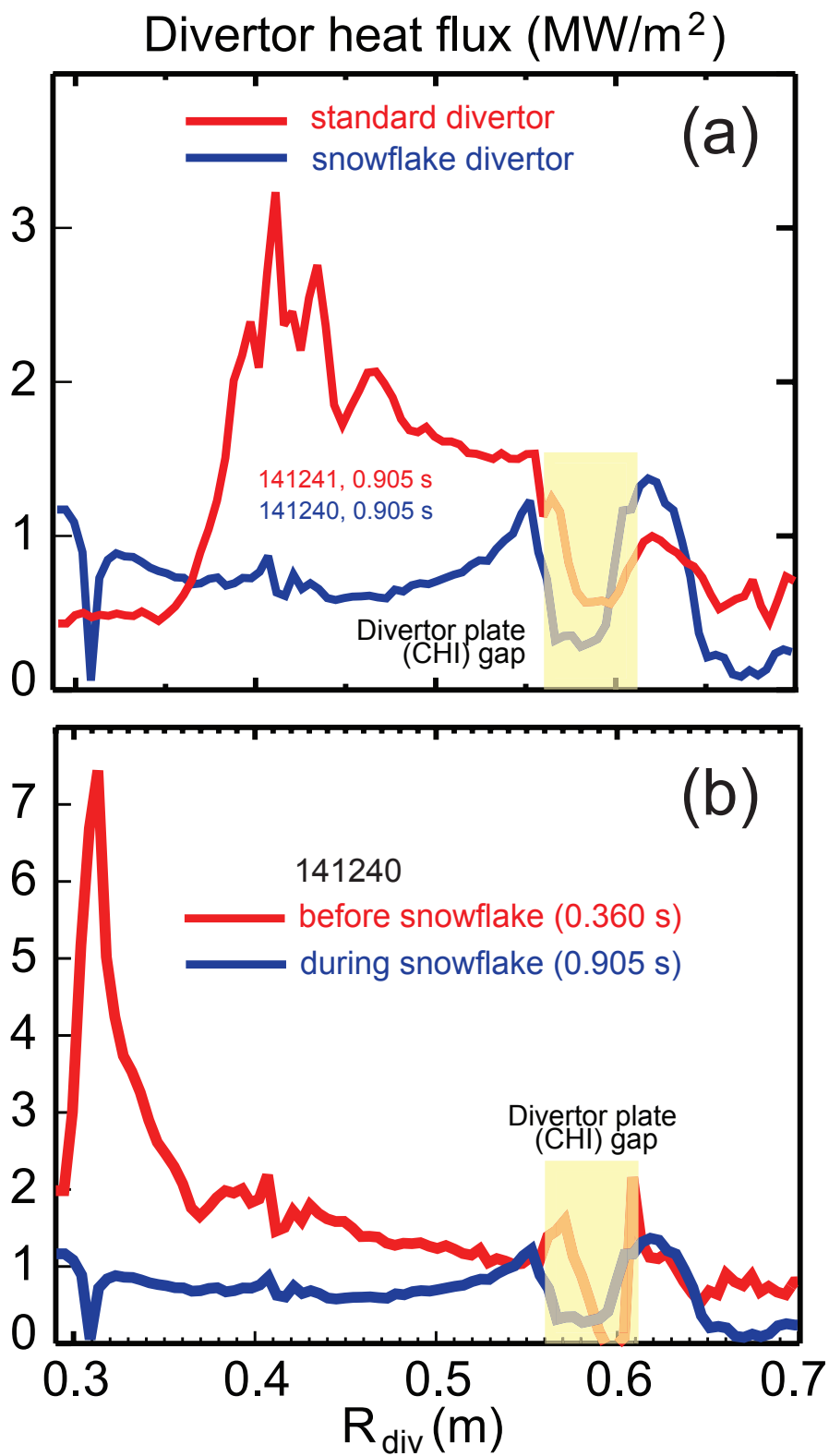


Figure 26. (a) Peak heat flux in a standard divertor configuration in NSTX (red) compared to the snowflake divertor configuration (blue), and (b) comparison of peak heat fluxes in same discharge with high-triangularity lower-single-null divertor configuration before snowflake (red) and during snowflake (blue).